regions at the active site of enzymes with a cobalt(III) complex, as an extension of the present study, which is also encouraged by the success of optical spectra in the identification of the ligands bound to cobalt(III) in the active sites of enzymes.[52]

There are many other applications to which the considerable sensitivity of the cobalt-59 chemical shift to its environment can be put; we hope to report on some of these in the near future.

Acknowledgment. The spectrometer used in this study was purchased with Grants 2.4504.78 and 21.420D from Fonds de la Recherche Fondamentale Collective, Brussels. We are grateful to Professor Robert J. Kurland for his helpful comments about activity coefficients.

(52) Navon, G.; Shinar, H. *Inorg. Chim. Acta* **1980**, *46*, 51-5.

NMR Relaxation Parameters in Molecules with Internal Motion: Exact Langevin Trajectory Results Compared with Simplified Relaxation Models†

Ronald M. Levy,* Martin Karplus,‡ and Peter G. Wolynes§

Contribution from the Departments of Chemistry, Harvard University, Cambridge, Massachusetts 02138, Rutgers University, New Brunswick, New Jersey 08903, and the University of Illinois, Urbana, Illinois 61801. *Received January 19, 1981*

Abstract: The interpretation of NMR relaxation experiments on flexible molecules is explored by use of stochastic dynamics trajectories. The effect of internal motion on the relaxation parameters (T_1, T_2, and NOE) of simple alkanes and of aliphatic side chains of proteins is determined. The correlation functions and spectral densities required for the evaluation of ^{13}C NMR relaxation times are evaluated from trajectories lasting up to 100 ns and the results are compared with the predictions of simplified analytical models for the motion. It is shown that for small molecules tumbling in the motional narrowing limit it is possible to approximately separate the NMR relaxation into contributions from tumbling and internal motions. For butane and heptane in aqueous solution, the spin-lattice relaxation times (T_1) are predicted and the gradient in relaxation times along the heptane chain is found to be close to that observed in the pure liquid. Detailed trajectory results are presented for ^{13}C relaxation of an alkane side chain on macromolecules. Wigner functions are used to express the side chain relaxation with respect to the coordinate frame embedded in the macromolecule. Uncoupling the motions about the individual side chain internal rotation axes or introduction of the independent lattice jump model for the motion is shown to describe incorrectly the short-time and long-time relaxation behavior. Nevertheless, for short side chains with barriers to rotation on the order of 3 kcal/mol, both models provide a good approximation for the ^{13}C NMR relaxation. This suggests that the models can be used for the interpretation of NMR experiments on lipids and aliphatic amino acid side chains protruding into solution, although errors are expected when the motion of the chain under consideration is constrained b the rest of the system.

I. Introduction

Nuclear magnetic resonance relaxation measurements provide an important probe of the dynamics of molecules since the spin-lattice (T_1) and spin-spin (T_2) relaxation times and the NOE enhancement factor (η) are all functions of the thermal motions. Carbon-13 NMR of protonated carbons is particularly well-suited for the study of dynamics because the relaxation is dominated by the fluctuating dipolar interactions between ^{13}C nuclei and directly bonded protons. Applications of ^{13}C NMR have been made to the dynamics of small molecules in solution,[1-6] polymers,[7-13] and molecules of biological interest including lipids[14-16] and proteins.[17-23] Since the motions of molecules with many internal degrees of freedom (e.g., macromolecules) are complicated, the interpretation of NMR measurements for such systems is often not unique. Empirical rules have been developed to fit the relaxation data to the molecular tumbling time combined with internal segmental motions.[6-8] Alternatively, the experimental results have been interpreted in terms of analytically tractable descriptions of the dynamics based on continuous diffusion,[9,24] restricted diffusion,[25-28] and lattice jump models.[24,26,29,30] While it is usually possible to fit the experimental results in this way, the data in themselves generally are not sufficient to determine whether a model gives the correct description of the dynamics.

A powerful method for testing relaxation models is provided

* Address correspondence to this author at Rutgers University.

† Supported in part by grants from the National Science Foundation, the National Institutes of Health, the Rutgers University Research Council, and BRSG.

‡ Harvard University.
§ University of Illinois.

(1) K. Kuhlman, D. Grant, and R. Harris, *J. Chem. Phys.*, **52**, 3439 (1970).
(2) J. R. Lyerla, Jr., and D. Grant, *J. Phys. Chem.*, **76**, 3213 (1972).
(3) D. Bauer, G. Alms, J. Brauman, and R. Pecora, *J. Chem. Phys.*, **61**, 2255 (1974).
(4) J. R. Lyerla, Jr., and G. C. Levy, *Top. Carbon-13 NMR Spectrosc.*, **1**, 79 (1974).
(5) J. Jonas in "Proceedings of the Nato ASI on High Pressure Chemistry", Reidel, Dordrecht, 1978.
(6) D. Doddrell and A. Allerhand, *J. Am. Chem. Soc.*, **93**, 1558 (1971).
(7) T. M. Connor, Trans. *Faraday Soc.*, **60**, 1579 (1963).
(8) J. Schaefer, *Macromolecules*, **6**, 882 (1973).
(9) Y. K. Levine, N. Birdsall, A. G. Lee, J. C. Metcalfe, P. Partington, and G. C. K. Roberts, *J. Chem. Phys.*, **60**, 2890 (1974).
(10) J. R. Lyerla, Jr., H. M. McIntyre, and D. A. Torchia, *Macromolecules*, **7**, 11 (1974).
(11) J. R. Lyerla, Jr., and T. T. Horikawa, *J. Phys. Chem.*, **80**, 1106 (1976).
(12) G. C. Levy, D. E. Axelson, R. Schwartz, and J. Hochmann, *J. Am. Chem. Soc.*, **100**, 410 (1978).
(13) D. Canet, J. Brondeau, H. Nery, and J. P. Marchol, *Chem. Phys. Lett.*, **72**, 184 (1980).
(14) A. G. Lee, N. J. M. Birdsall, J. C. Metcalfe, G. B. Warren, and G. C. K. Roberts, *Proc. R. Soc. London, Ser. B*, **193**, 253 (1976).
(15) P. Godici and F. Landsberger, *Biochemistry*, **14**, 3927 (1975).
(16) D. Bocian and S. Chan, *Annu. Rev. Phys. Chem.*, **29**, 307 (1978).
(17) E. Oldfield, R. Norton, and A. Allerhand, *Biochemistry*, **250**, 6368 (1975).
(18) E. Oldfield, R. Norton, and A. Allerhand, *Biochemistry*, **250**, 6381 (1975).
(19) R. Visscher and F. R. N. Gurd, *J. Biol. Chem.*, **250**, 2238 (1975).

0002-7863/81/1503-5998$01.25/0

by computer-generated trajectories that make use of realistic potentials to simulate the motion of the system of interest. From such trajectories, the time-dependent correlation functions can be determined and T_1, T_2, and η can be calculated. Thus, the trajectory provides simultaneously a complete knowledge of the dynamics and exact values of the NMR parameters. It is now possible to proceed by using the calculated values of T_1, T_2, and η as "experimental" quantities and fitting the various models to them. The resulting model dynamics can then be compared with the exact dynamics from the trajectory to determine how well the former corresponds to the latter. Alternatively, we can use the trajectory results directly to evaluate the model parameters and then compare the values of T_1, T_2, and η obtained from the models with the exact values from the trajectories. The limitation of experimental studies, in which the dynamics of the molecules is not known, is thus obviated by the trajectory analysis. Also, the results of the trajectory studies may be compared directly with experiment without recourse to simplified theories. The effect of solvent can be introduced by including solvent molecules in the dynamics or by using stochastic dynamics techniques.

Recently, there have been published a number of molecular dynamics simulations of polymer chains.[31-40] It is the object of the present paper to employ the results of one such simulation[34,40] for the analysis of experimental and theoretical NMR studies of polymer dynamics. In that simulation the diffusive Langevin equation of motion was applied to butane and heptane to simulate the equilibrium and dynamic properties in aqueous solutions for times up to 100 ns. Section II outlines the methodology employed to extract the NMR parameters from these alkane chain trajectories. The trajectories are used in Section III to evaluate the relaxation times for short alkane chains in the motional narrowing limit and the results are compared with experiment and with simplified models. In Section IV the dynamics of a side chain protruding from a macromolecule is analyzed and the heptane trajectories are employed to critically examine a lattice jump model for the relaxation.

II. Methodology

In this section, we briefly outline the method used for obtaining the alkane trajectories and then present in some detail the procedure for determining NMR relaxation parameters from these trajectories. It is shown also how the trajectory results can be applied to some of the simplified dynamical models that have been used to interpret NMR relaxation data.

a. Exact Calculation of NMR Parameters. Butane and heptane trajectories were obtained from extended atom models of these alkanes, in which the CH_3 and CH_2 groups are represented as spheres acting as point centers of frictional resistance.[34] The trajectories were constructed by simultaneously integrating in Cartesian coordinates the diffusive Langevin equations of motion for the extended-atom units of the alkane chains;[34] the complete Langevin equation has the form

$$m_i \frac{d\vec{v}_i}{dt} = -\zeta_i \vec{v}_i + \vec{F}_i + \vec{A}_i \qquad (1a)$$

where m_i, $\vec{v}_i$, and ζ_i are the mass, velocity, and friction constant of the ith particle, $\vec{F}_i$ is the systematic force acting on the ith particle due to the potential of mean force, and $\vec{A}_i$ is the Brownian random force term. In the diffusive limit, eq 1a can be integrated to obtain an expression for the displacement vector, $\vec{r}_i$,

$$\vec{r}_i(t + \Delta t) = \vec{r}_i(t) + [\vec{F}_i(t)/\zeta_i]\Delta t + \Delta\vec{r}_i(t) \qquad (1b)$$

where Δt is the time interval and $\Delta\vec{r}_i(t)$ is the random displacement due to the force $\vec{A}_i$. The force $\vec{F}_i$, which is obtained from a given potential, depends, in general, on the coordinates of all of the particles. For calculating the butane and heptane trajectories, a potential of mean force was employed; it is composed of intramolecular van der Waals and torsional potential terms plus an aqueous solvent contribution.[34] The results simulate alkanes or hydrophobic amino acid side chains such as leucine and isoleucine dissolved in water. The barrier to rotation arising from the torsional contribution to the potential about each of the internal single bonds is ~3.0 kcal/mol (~5 kT at room temperature). Due to the presence of the van der Waals term, the conformational sequence gauche (+), gauche (−) along the chain is energetically forbidden.

For the analysis of NMR relaxation in the motional narrowing limit (Section III), a 40 ns portion of the complete 90 ns butane trajectory and a 6 ns portion of the complete 21 ns heptane trajectory were chosen.[34] Cartesian coordinate values at 1 ps intervals along the trajectories were employed in the calculations. The complete 21 ns heptane trajectory was used in Section IV, where we focus on the relaxation of side chains attached to tumbling macromolecules. The time interval between coordinates in the latter calculation was 5 ps.

The NMR relaxation parameters probe angular correlation functions of the relaxing nucleus. These correlation functions and their Fourier transforms, the spectral densities, can be obtained directly from the alkane trajectories, which provide the complete chain dynamics in the diffusive limit. For a ^{13}C nucleus in an alkane chain, the dynamical quantities of interest are the spherical polar coordinates (with respect to a laboratory frame) of the C–H internuclear vectors. The well-known relations between the NMR relaxation parameters T_1, T_2, and η and the spectral densities for the case of dipolar relaxation involving two different spin $^1/_2$ nuclei are[41,42]

$$\frac{1}{T_1} = \frac{N\hbar^2\gamma_C^2\gamma_H^2}{r^6}\frac{4\pi}{10}\{J_0(\omega_0 - \omega_H) + 3J_1(\omega_C) + 6J_2(\omega_C + \omega_H)\} \qquad (2)$$

$$\frac{1}{T_2} = \frac{N\hbar^2\gamma_C^2\gamma_H^2}{r^6}\frac{4\pi}{20}\{4J_0(0) + J_0(\omega_C - \omega_H) + 3J_1(\omega_C) + 6J_1(\omega_H) + 6J_2(\omega_C + \omega_H)\} \qquad (3)$$

$$\eta = \frac{\gamma_H}{\gamma_C}\left[\frac{6J_2(\omega_C + \omega_H) - J_0(\omega_C - \omega_H)}{J_0(\omega_C - \omega_H) + 3J_1(\omega_C) + 6J_2(\omega_C + \omega_H)}\right] \qquad (4)$$

where γ_C, γ_H and ω_C, ω_H are the gyromagnetic ratios and Larmor frequencies of the ^{13}C and ^1H nuclei, r is the C–H bond distance, and N is the number of protons directly bonded to the relaxing carbon nucleus. The spectral densities, $J_m(\omega)$, are the Fourier

(20) W. C. Jones, Jr., T. M. Rothgeb, and F. R. N. Gurd, *J. Biol. Chem.*, 7452 (1976).
(21) R. J. Wittebort, T. M. Rothgeb, A. Szabo, and F. R. N. Gurd, *Proc. Natl. Acad. Sci. U.S.A.*, **76**, 1059 (1979).
(22) L. W. Jelinski and D. Torchia, *J. Mol. Biol.*, **133**, 45 (1979).
(23) L. W. Jelinski and D. Torchia, *J. Mol. Biol.*, **138**, 255 (1980).
(24) D. Wallach, *J. Chem. Phys.*, **47**, 3258 (1967).
(25) R. J. Wittebort, A. Szabo, and F. R. N. Gurd, *J. Am. Chem. Soc.*, **102**, 5723 (1980).
(26) R. J. Wittebort and A. Szabo, *J. Chem. Phys.*, **69**, 1722 (1978).
(27) R. E. London and J. Avitable, *J. Am. Chem. Soc.*, **100**, 7159 (1978).
(28) O. W. Howarth, *Faraday Discuss. Chem. Soc., Part 2*, **75**, 863 (1979).
(29) R. E. London and J. Avitable, *J. Am. Chem. Soc.*, **99**, 7765 (1977).
(30) A. Tsutsumi and C. Chachaty, *Macromolecules*, **12**, 429 (1979).
(31) J. P. Ryckaert and A. Bellemans, *Faraday Discuss. Chem. Soc.*, **66**, 95 (1978).
(32) J. H. Weiner and M. R. Pear, *Macromolecules*, **10**, 317 (1977).
(33) T. Weber, *J. Chem. Phys.*, **70**, 4277 (1979).
(34) R. M. Levy, M. Karplus, and J. A. McCammon, *Chem. Phys. Lett.*, **65**, 4 (1979).
(35) M. Fixman, *J. Chem. Phys.*, **69**, 1538 (1978).
(36) E. Helfand, Z. R. Wasserman, and T. A. Weber, *J. Chem. Phys.*, **70**, 2016 (1979).
(37) G. T. Evans and D. C. Knauss, *J. Chem. Phys.*, **71**, 2255 (1979).
(38) G. T. Evans and D. C. Knauss, *J. Chem. Phys.*, **72**, 1504 (1980).
(39) J. A. Montgomery, S. L. Holmgren, and D. Chandler, *J. Chem. Phys.*, **73**, 3688 (1980).
(40) R. M. Levy, "Diffusive Dynamics of Alkane Chains", in 1978 CECAM Workshop Report on Stochastic Dynamics, Universite de Paris.
(41) A. Abragaham, "The Principles of Nuclear Magnetism", Oxford University Press, London, 1978.
(42) D. Doddrell, V. Glushko, and A. Allerhand, *J. Chem. Phys.*, **56**, 3683 (1972).

transforms of the second-order spherical harmonics, $Y_m^2(\theta,\phi)$, given by

$$J_m(\omega) = \int_0^\infty \langle Y_m^2(\theta(t)\phi(t)) Y_m^{2*}(\theta(0)\phi(0))\rangle \cos \omega t \, dt \quad (5)$$

where the spherical-harmonic time correlation function is defined as the ensemble average,[43]

$$\langle Y_m^2(\theta(t)\phi(t)) Y_m^{2*}(\theta(0)\phi(0))\rangle = \int d\theta \, d\phi \int d\theta' \, d\phi' \, Y_m^2(\theta,\phi) G(\theta,\phi,t;\theta',\phi',0) Y_m^{2*}(\theta'\phi') \quad (6)$$

Here $G(\theta,\phi,t;\theta',\phi',0)$ is the conditional probability that a CH vector has spherical polar coordinates (θ,ϕ) at times t given that they were equal to (θ',ϕ') at time 0. The spherical-harmonic time correlation functions are obtained from the alkane trajectories by replacing the ensemble average (eq 6) with a time average. This time average is determined by taking the function $Y_m^2(\theta(s)\phi(s))$ at time s, multiplying it by $Y_m^{2*}(\theta(s+t)\phi(s+t))$, the value taken by Y_m^{2*} after the system has evolved for an additional time t, evaluating such products for a representative set of initial times, s, and averaging the results. Since the orientation of the laboratory z axis is arbitrary for freely rotating molecules, the angular correlations and their spectral densities are independent of subscript m. This property supplies one test of whether the alkane trajectories have been run long enough to establish an equilibrium distribution of configurations. Another test of the equivalence of the time and ensemble averages is provided by the equal-time correlation functions, $\langle Y_m^2(\theta(s)\phi(s)) Y_m^{2*}(\theta(s)\phi(s))\rangle$. Their time averages must satisfy the ensemble normalization requirement,

$$\langle Y_m^2(\theta(0)\phi(0)) Y_m^{2*}(\theta(0)\phi(0))\rangle = 1/4\pi \quad (7)$$

Both of these conditions are employed to test the trajectory results in Section III.

Once the correlation functions (eq 6) have been evaluated from the time integral over the trajectory, the spectral densities are obtained by numerical Fourier transformation, as indicated in eq 5. The resulting values of $J_m(\omega)$ are then introduced into eq 2-4 to determine the NMR parameters.

b. Relaxation Models. The ^{13}C NMR spectra of low molecular weight species in solution have tumbling times that are much smaller than the reciprocal of the Larmor frequencies of current spectrometers. Consequently, the resonances of such systems are observed in the motional narrowing limit $[(\omega_C\tau)^2 \ll 1]$, where the relaxation time τ is the time integral of the angular correlation function,

$$\tau \equiv \int_0^\infty \langle Y_m^2(\theta(t)\phi(t)) Y_m^{2*}(\theta(0)\phi(0))\rangle \, dt \quad (8)$$

In the motional narrowing limit, the NMR relaxation times T_1 and T_2 are equal and independent of the Larmor frequency and the ^{13}C dipolar NOE is maximal;[1,42] that is, eq 2-4 reduce to

$$\frac{1}{T_1} = (4\pi\tau)\frac{N\hbar^2\gamma_C^2\gamma_H^2}{r^6} \quad (9)$$

$$T_2 = T_1 \quad (10)$$

$$\mathrm{NOE} = 1 + \eta = 2.99 \quad (11)$$

For rigid spherical molecules in solution, the rotational motion is described by the angular Debye diffusion equation and the second-order spherical harmonics decay as a single exponential[43] with relaxation time $\tau = 1/(6D)$, where D is the rotational diffusion coefficient. For flexible molecules a distribution of relaxation times is required to describe the motion of a given C-H vector. It is common to associate, with each carbon in such a system, an effective relaxation time, τ_{eff}, which may be thought of as a weighted average of the distribution of relaxation times. Empirically, τ_{eff} has been separated into contributions from molecular tumbling and segmental motions,[6,10,11]

$$\frac{1}{\tau_{eff}} = \frac{1}{\tau_0} + \frac{1}{\tau_i} \quad (12)$$

where τ_0 is the molecular tumbling time, and τ_i is the segmental motion relaxation time for the ith carbon. To derive eq 12 by separating the overall tumbling and internal motions, we consider a local coordinate system centered on the relaxing nucleus and determine its motion relative to a coordinate frame embedded in the molecule. To express the angular correlation functions (eq 6) in terms of these coordinate systems, we introduce Wigner rotation matrices.[44] The resulting expression is (see Appendix A for details),

$$\langle Y_m^2(\theta(t)\phi(t)) Y_m^{2*}(\theta(0)\phi(0))\rangle = \sum_{\substack{aa' \\ bb'}} \langle [\mathbf{D}_{ma}^{2*}(\Omega_0(t))\mathbf{D}_{ma'}^2(\Omega_0(0))] \times [\mathbf{D}_{ab}^{2*}(\Omega_i(t))\mathbf{D}_{a'b'}^2(\Omega_i(0))]\rangle Y_b^2(\theta_{mol},\phi_{mol}) Y_{b'}^{2*}(\theta_{mol},\phi_{mol}) \quad (13)$$

where $\mathbf{D}_{ab}^2(\Omega)$ is the Wigner rotation matrix, $\Omega_0(t)$ are the Euler angles for the transformation from the laboratory to the molecular coordinate system, and $\Omega_i(t)$ are the Euler angles for the transformation from the molecular coordinate system to the local coordinates centered on the ith relaxing nucleus. The angles $(\theta_{mol},\phi_{mol})$ are the time-independent spherical polar coordinates of the C-H internuclear vector in the local coordinate system. The assumption that tumbling and internal motions are independent leads to the expression

$$\sum_{\substack{aa' \\ bb'}} \langle [\mathbf{D}_{ma}^{2*}(\Omega_0(t))\mathbf{D}_{ma'}^2(\Omega_0(0))] \times [\mathbf{D}_{ab}^{2*}(\Omega_i(t))\mathbf{D}_{a'b'}^2(\Omega_i(0))]\rangle Y_b^2(\theta_{mol},\phi_{mol}) Y_{b'}^{2*}(\theta_{mol},\phi_{mol}) \approx \sum_{\substack{aa' \\ bb'}} \langle \mathbf{D}_{ma}^{2*}(\Omega_0(t))\mathbf{D}_{ma'}^2(\Omega_0(0))\rangle \times \langle \mathbf{D}_{ab}^{2*}(\Omega_i(t))\mathbf{D}_{a'b'}^2(\Omega_i(0))\rangle Y_b^2(\theta_{mol},\phi_{mol}) Y_{b'}^{2*}(\theta_{mol},\phi_{mol}) \quad (14a)$$

For a molecule undergoing isotropic rotational diffusion, the tumbling correlation function decays as a single exponential with relaxation time τ_0 and eq 14a is reduced to

$$\langle Y_m^2(\theta(t)\phi(t)) Y_m^{2*}(\theta(0)\phi(0))\rangle \approx \sum_{abb'} \frac{e^{-t/\tau_0}}{5} \langle \mathbf{D}_{ab}^{2*}(\Omega_i(t))\mathbf{D}_{ab'}^2(\Omega_i(0))\rangle \times Y_b^2(\theta_{mol},\phi_{mol}) Y_{b'}^{2*}(\theta_{mol},\phi_{mol}) \quad (14b)$$

If the internal motion correlation function also decays as a single exponential (as it would if there were free diffusion), we have

$$\langle \mathbf{D}_{ab}^{2*}(\Omega_i(t))\mathbf{D}_{ab'}^2(\Omega_i(0))\rangle \sim e^{-t/\tau_i}\delta_{bb'} \quad (15)$$

with τ_i related to the internal rotational diffusion constant. Introduction of this result into eq 14b permits one to obtain an expression of the form of eq 12 for τ_{eff}.

In order to introduce more sophisticated relaxation models, it is convenient to describe the decay of the angular correlation function in terms of a set of parameters determined by the internal chain dynamics. If the ith nucleus is separated from the center of molecular tumbling by N internal rotation axes (see Figure 1), we can write eq 13 in the general form (see Appendix A),[24]

$$\langle Y_m^2(\theta(t)\phi(t)) Y_m^{2*}(\theta(0)\phi(0))\rangle = \sum_{\substack{a,b_1,b_2\ldots b_N \\ a',b_1',b_2'\ldots b_N'}} \langle [\mathbf{D}_{ma}^{2*}(\Omega_0(t))\mathbf{D}_{ma'}^2(\Omega_0(0))] \times [\mathbf{D}_{ab_1}^{2*}(\Omega_1(t))\mathbf{D}_{a'b_1'}^2(\Omega_1(0))][\mathbf{D}_{b_1b_2}^{2*}(\Omega_2(t))\mathbf{D}_{b_1'b_2'}^2(\Omega_2(0))]\ldots \times [\mathbf{D}_{b_{N-1}b_N}^{2*}(\Omega_N(t))\mathbf{D}_{b_{N-1}'b_N'}(\Omega_N(0))]\rangle \times Y_{b_N}^2(\theta_{mol},\phi_{mol}) Y_{b_N'}^{2*}(\theta_{mol},\phi_{mol}) \quad (16)$$

The simplest theory assumes that the rotational motions about the bonds of the chain are independent. The angular correlation function of eq 16 then reduces to a sum over a product of cor-

(43) B. Berne and R. Pecora, "Dynamic Light Scattering", Wiley, New York, 1976, Chapter 7.

(44) D. M. Brink and G. R. Satchler, "Angular Momentum", Oxford University Press, London, 1971.

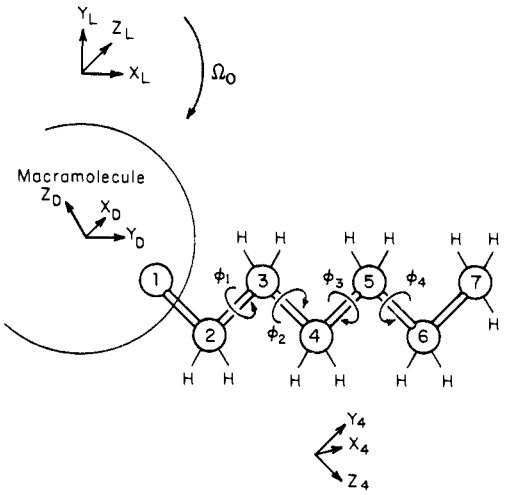

Figure 1. Schematic representation of a side chain with four internal rotational angles attached to a tumbling macromolecule. The laboratory coordinate system, molecular tumbling coordinate system, and a coordinate system attached to C_4 are labeled.

relation functions determined by the motions about the successive rotational axes (see Appendix A).[9,21,29] If, in addition, isotropic rotational diffusion is assumed as in eq 14b, we obtain

$$\langle Y_0^2(\theta(t)\phi(t))Y_0^{2*}(\theta(0)\phi(0))\rangle = \sum_{\substack{a,b_1,b_2,b_N \\ b_1',b_2',b_N'}} \frac{e^{-t/\tau_0}}{5}\langle \mathbf{D}_{ab_1}^{2*}(\Omega_1(t))\mathbf{D}_{ab_1'}^{2}(\Omega_1(0))\rangle \times \langle \mathbf{D}_{b_1b_2}^{2*}(\Omega_2(t))\mathbf{D}_{b_1'b_2'}^{2}(\Omega_2(0))\rangle \ldots \times \langle \mathbf{D}_{b_{N-1}b_N}^{2*}(\Omega_N(t))\mathbf{D}_{b_{N-1}'b_N'}^{2}(\Omega_N(0))\rangle \times Y_{b_N}^{2}(\theta_{mol},\phi_{mol})Y_{b_N'}^{2*}(\theta_{mol},\phi_{mol}) \quad (17)$$

In the free internal diffusion model, rotational barriers are neglected and each of the time correlation functions of eq 17 relaxes exponentially as in eq 15 with a rate constant identified as the rotational diffusion constant about the corresponding bond of the chain. It is generally assumed that except for the internal rotation axes, the molecule is rigid (i.e., the bond lengths and bond angles are fixed).

More realistic models of NMR relaxation in polymers take account of the presence of intrinsic torsional barriers and of excluded volume effects. A class of NMR relaxation problems where such effects are likely to be very important deals with the relaxation of amino acid side chains in the interior of proteins.[21-29] If the side chain librational motion is dominated by steric interactions with the rest of the protein, restricted diffusion models may be appropriate.[25,26] In this approach, one still assumes that the internal degrees of freedom diffuse independently but introduces steric interactions that restrict the allowed values of the internal rotation angles. Application of the model to relaxation data makes it possible to determine angular bounds on the internal motions of amino acid side chains. Another type of analytic model, which has been applied to hydrocarbon chains in membranes and in solution, is the so-called "jump" model.[26,27] For many systems, the intrinsic torsional barriers to isomerization are so large that the actual transit time between stable conformations is very short compared with the time the chain spends close to the potential minima; "jumping" is an idealization of this kind of motion. Further, in a lattice jump model transitions among configurations are specified by a master equation so that only sterically allowed configurations are included. The lattice jump model also can take account of concerted chain motions involving simultaneous multiple isomerizations by appropriate choice of the transition matrix. In practice, there have been few attempts to interpret experimental NMR relaxation data within the context of a complete lattice jump model because the number of adjustable parameters rapidly becomes unwieldly. For the hydrocarbon relaxation problem, it has been common to employ the model with the product approximation for the relaxation (eq 17); this omits excluded volume effects and

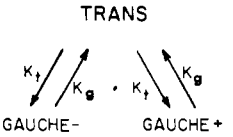

Figure 2. Schematic representation of trans, gauche (+), and gauche (−) configurations and rate constants K_t for jumping from trans to gauche (+) or (−) and K_g for jumping from gauche (+) or (−) to trans states.

the possibility of concerted motions. Figure 2 exhibits the rate matrix associated with each internal degree of freedom for this simple case. Each carbon–carbon bond is allowed to jump between three states, trans, gauche (+), and gauche (−). The rate constant for jumping from the trans (τ) to gauche (g^+, g^-) states is K_T and the inverse rate constant is K_G. Direct jumps between gauche (+) and gauche (−) states are forbidden. However, since the rotational motions about the bonds are assumed to be independent, physically forbidden gauche (+), gauche (−) conformers are allowed. For this simplified lattice jump model the correlation functions for each of the internal degrees of freedom (eq 17) can be written as a sum over the conditional probabilities for the allowed transitions in the form (Appendix B)

$$\langle \mathbf{D}_{ab}^{2*}(\Omega(t))\mathbf{D}_{a'b'}^{2}(\Omega(0))\rangle = d_{ab}^{2}(\beta)d_{a'b'}^{2}(\beta)\sum_{\phi=\tau,g^-,g^+}\sum_{\phi=\tau,g^-,g^+} e^{i[b\phi-b'\phi']}P_0(\phi')P(\phi t|\phi' 0) \quad (18)$$

The d_{ab}^2 are real reduced Wigner matrix elements with β the complement of the rigid CCC bond angle, $P(\phi t|\phi' 0)$ is the conditional probability that a rotational angle is ϕ at time t, given that it was ϕ' at time 0, and $P_0(\phi')$ is the equilibrium probability of a ϕ' state. In Appendix B explicit expressions for the conditional probabilities are derived in terms of the eigenvalues and eigenvectors of the rate matrix.

c. Comparison of Trajectory and Model Calculations. The trajectory results are compared with analytic models for two types of systems; the first corresponds to a hydrocarbon chain in aqueous solution (Section III) and the second to an aliphatic amino acid side chain that is protruding into solution from a protein (Section IV).

The complete trajectory calculation for the hydrocarbon is exact within the model used for the potential and the stochastic treatment of the solvent effect; that is, both small oscillations within a potential well and jumps over the internal rotation barrier are included, as are any contributions from excluded volume effects and concerted motions that may occur. Comparison between the trajectory results for the NMR parameters and various simplified models are made in Section III. In addition, the calculations are employed in an analysis of experimental NMR data available for hydrocarbon chains.

To utilize the heptane trajectory in a model study of an amino acid side chain protruding from a macromolecule, it is necessary to introduce the assumption made in eq 14 that the overall molecular tumbling and the internal side chain motions are independent. Also, in the present study, no account is take of possible interactions between the side chain and the rest of the protein, which could restrict the side chain motions. With these simplifications, comparisons can be made between the "exact" results for the side chain motion obtained from the trajectories and simplified models; in particular, the lattice jump model is studied in some detail.

In Section IV, the heptane trajectory is used to evaluate T_1, T_2, and NOE for a model amino acid side chain with four internal rotational angles. Figure 1 shows the four rotational angles and indicates the nature of the three types of coordinate systems that are used to define the configurations of the chain; that is, the laboratory system, the macromolecular system with respect to which the overall tumbling is defined, and the four local coordinate frames associated with the internal degrees of freedom. For the analysis, the coordinate frame centered on C_2 is assumed to be rigidly attached to the macromolecule, which is tumbling isotropically with relaxation time τ_0. The orientations of the C_2–H internuclear vectors are fixed by specifying the orientation of the

Table I. Initial Values of Angular Correlation Functions[a]

butane[b]	$\langle Y_0^1(0)$-$Y_0^1(0)\rangle$	$\langle Y_0^2(0)$-$Y_0^{2*}(0)\rangle$	$\langle Y_1^2(0)$-$Y_1^{2*}(0)\rangle$	$\langle Y_2^2(0)$-$Y_2^{2*}(0)\rangle$
C1–C2	0.0802	0.0802	0.0796	0.0792
C2–C3	0.0791	0.0802	0.0787	0.0801
C3–C4	0.0781	0.0795	0.0785	0.0808
C2–H	0.0786	0.0776	0.0773	0.0774
C3-H	0.0792	0.0780	0.0775	0.0769
mean	0.0790	0.0791	0.0783	0.0789
σ[c]	±0.0007	±0.0012	±0.0009	±0.0017
heptane[d]	$\langle Y_0^1(0)$-$Y_0^{1*}(0)\rangle$	$\langle Y_0^2(0)$-$Y_0^{2*}(0)\rangle$	$\langle Y_1^2(0)$-$Y_1^{2*}(0)\rangle$	$\langle Y_2^2(0)$-$Y_2^{2*}(0)\rangle$
C1–C2	0.0715	0.0695	0.0795	0.0847
C2–C3	0.0822	0.0831	0.0794	0.0780
C3–C4	0.0745	0.0727	0.0799	0.0827
C4–C5	0.0791	0.0813	0.0780	0.0803
C5–C6	0.0728	0.0740	0.0777	0.0843
C6–C7	0.0847	0.0848	0.0804	0.0761
C2-H	0.0869	0.0846	0.0793	0.0716
C3-H	0.0788	0.0799	0.0760	0.0774
C4-H	0.0834	0.0850	0.0761	0.0745
C5-H	0.0847	0.0801	0.0804	0.0725
C6-H	0.0755	0.0749	0.0780	0.0789
mean	0.0795	0.0791	0.0786	0.0783
σ[c]	±0.0053	±0.0055	±0.0016	±0.0045

[a] The ensemble average value is $\langle Y_m^{2*}(\theta(0)\phi(0)Y_m^2(\theta(0)\phi(0))\rangle = 1/4\pi = 0.0796$. [b] 40 ns trajectory. [c] Standard deviation. [d] 6 ns trajectory.

macromolecule. In order to locate the C_3–H internuclear vectors, both the orientation of the macromolecule and the first rotational angle, ϕ_1, must be specified. The C_4–H vectors are fixed by specifying (Ω_0,ϕ_1,ϕ_2) and so on; all the dynamical variables $(\Omega_0,\phi_1,\phi_2,\phi_3,\phi_4)$ are required to specify the orientation of the C_6–H internuclear vectors. Since the extended-atom alkane model does not contain explicit protons, the C–H internuclear vectors are constructed from $(C_{i-1}$–C_i–$C_{i+1})$ coordinates by assuming tetrahedral bonding to C_i; the C–H vibrations are excluded. Only carbons C_2 through C_6 are considered since the C_7 methyl protons cannot be located from an extended-atom alkane model. The macromolecular tumbling contributes to the relaxation of all of the carbons (C_2 through C_6), while the internal dynamics contributes progressively to atoms C_3 through C_6; that is, motions about the C_2–C_3 axis reorient not only the C_3–H vectors but all of the C–H vectors from atoms C_3 through C_6. The NMR relaxation parameters are calculated from eq 2-4; eq 13-17 are used to evaluate the correlation functions. The numerical results required for calculating the correlation functions are obtained from the heptane trajectory; the method used for evaluating the correlation function with the product approximation is given in Appendix C. Results obtained with assumed macromolecular tumbling times of 1, 10, and 100 ns are compared. The NMR properties obtained from eq 14b, where the product approximation is applied only to factor out the tumbling motion and correlations between the internal motions are explicitly included, are compared with the results of the complete product approximation (eq 17). These two sets of calculations for the NMR parameters are then compared with those obtained from the independent lattice jump model. For the latter, only the isomerization rate constants K_T and K_G for each of the rotational angles are required. They are obtained from the heptane trajectory, as previously reported,[34,40] by analyzing the time dependence of the fluctuations in the trans and gauche states along the chain.

III. NMR Relaxation of Model Alkanes in the Motional Narrowing Limit

In this section we employ the stochastic trajectory results for butane and heptane to analyze the contributions to the carbon-13 relaxation times in simple alkanes. We first examine certain properties of the calculated angular correlation functions to determine whether the length of the trajectories is sufficient for convergence to the equilibrium values. We then analyze the calculated relaxation times and compare them with experimental trends. Finally, we examine some simplified models that have been proposed for interpreting alkane NMR data and test them by comparison with the trajectory results.

Table II. Relaxation Times of Butane Angular Correlation Functions[a]

bond	$\langle Y_0^{1*}(0)$-$Y_0^1(t)\rangle$ τ, ps	$\langle Y_0^{2*}(0)$-$Y_0^2(t)\rangle$ τ, ps	$\langle Y_1^{2*}(0)$-$Y_1^2(t)\rangle$ τ, ps	$\langle Y_2^{2*}(0)$-$Y_2^2(t)\rangle$ τ, ps
C1–C2	(18.5)[b] 16.0	5.7	5.6	5.8
C2–C3	(19.1) 16.9	6.1	5.9	6.4
C3–C4	(19.0) 15.9	6.0	5.6	5.8
C2-H	(7.6)[c] 8.1	(3.9)[c] 5.0	(4.0)[c] 4.9	(3.9)[c] 5.1
C3-H	(7.8) 8.3	(4.1) 5.2	(3.9) 4.8	(3.9) 5.1

[a] Relaxation time from least-squares fit of the relaxation to a single exponential over 10 ps, except as noted. [b] Least-squares fit to single exponential over 20 ps. [c] Least-squares fit to single exponential over 5 ps.

Table III. Relaxation Times of Heptane Angular Correlation Functions[a]

bonds	$\langle Y_0^1(0)$-$Y_0^1(t)\rangle$ τ, ps	$\langle Y_0^2(0)$-$Y_0^2(t)\rangle$ τ, ps	$\langle Y_1^{2*}(0)$-$Y_1^2(t)\rangle$ τ, ps	$\langle Y_2^{2*}(0)$-$Y_2^2(t)\rangle$ τ, ps
C1–C2	(39.3)[b] 33.4	13.4	14.7	15.9
C2–C3	(46.7) 42.2	16.5	15.1	16.5
C3–C4	(51.9) 49.8	17.6	19.6	20.2
C4–C5	(50.3) 46.7	18.1	16.9	18.3
C5–C6	(47.3) 41.6	16.5	17.2	18.3
C6–C7	(37.3) 35.7	13.7	12.9	13.5
C2-H	(32.6)[b] 29.1	12.6	11.7	11.9
C3-H	(31.5) 29.4	13.9	11.3	13.5
C4-H	(35.1) 33.1	15.1	11.6	13.3
C5-H	(33.8) 33.4	13.4	12.3	12.5
C6-H	(25.4) 23.3	9.9	12.9	12.7

[a] Relaxation time from least-squares fit of the relaxation to a single exponential over 10 ps, except as noted. [b] Fit to a single exponential over 20 ps.

a. Finite Time Averaging. The equal time correlation functions for the first- and second-order spherical harmonics are listed in Table I. The results for each of the carbon–carbon and carbon–proton bonds are very close to the ensemble average value $(1/4\pi)$, as given in eq 7. The largest deviation from the ensemble value is 13% (the Y_0^2 result for the C_1–C_2 internuclear vector of heptane). The mean values obtained by averaging over the results for the individual internuclear vectors are within 2% of the ensemble average and the standard deviations are all less than 10% of the mean values. That the butane standard deviations are smaller than those for heptane is as expected from the longer butane trajectory and the shorter butane relaxation times (see below).

It is of interest to compare the results presented in Table I with the Zwanzig-Ailawadi[45] estimate of the error in a time correlation function obtained by averaging over a single trajectory for a finite time. For a Gaussian random process, the relative error in the initial value of a time correlation function when compared with the ensemble value is of the order of $[2\tau/T]^{1/2}$, where τ is the relaxation time for the process and T is the duration of the trajectory. With use of the Zwanzig–Ailawadi formula and average values for the relaxation times of the second-order spherical harmonics for butane and heptane, the relative error in the results are predicted to be 2% or smaller for butane and 8% or smaller for heptane. These estimates are close to the observed standard deviations in the initial values.

For freely rotating molecules, the behavior of the second-order spherical harmonics with the same l must be independent of the value of m; this provides another test of whether the trajectory is of sufficient length. Tables II and III give the relaxation times

(45) R. Zwanzig and N. Ailawadi, *Phys. Rev.*, **182**, 280 (1969).

Table IV. Time Integral of Angular Correlation Function of C_6-H Vector and Exponential Relaxation Times

	$\int_0^\infty \langle Y_0^2(\theta(0)\phi(0)) \times Y_0^2(\theta(t)\phi(t))\rangle\, dt$, ps	relax time by single-exponential fit, ps
complete dynamics	0.68	9.9[b] (0.79)[a]
		10.5[c] (0.84)
tumbling and internal motions uncoupled	0.58	9.7[b] (0.77)
		11.7[c] (0.93)
tumbling relaxation only	1.21	13.0[b] (1.03)
		15.8[c] (1.26)
internal relaxation only		39.0[c] (3.1)
		40.1[d] (3.2)

[a] Values in parentheses are $1/4\pi$ times the exponential fit to correspond to the time integral (eq 8). [b] Least-squares fit to a single exponential over 10 ps. [c] Least-squares fit to a single exponential over 20 ps. [d] Least-squares fit to a single exponential over 50 ps.

for the spherical harmonics determined as indicated below. It is evident that for Y_m^2 the relaxation times do not depend on m; the largest deviations are found for the C–H vectors in heptane where the values differ by as much as 14% from the average result (e.g., for C_4–H in heptane).

b. Relaxation Time: Theory and Experiment In the motional narrowing limit applicable to the small alkanes, the ^{13}C dipolar spin–lattice relaxation times (T_1; see eq 9) are inversely proportional to the relaxation times (τ) of the second-order spherical harmonics. The computed relaxation times for each of the internuclear vectors of butane and heptane obtained from a least-squares fit of a single exponential to the decay of the calculated correlation functions are listed in Tables II and III, respectively. The fits to single exponentials are used here as estimates of the relaxation times. Since the relaxation is not due to isotropic rigid-body rotation, the single-exponential fit is approximate. From Tables II and III it is apparent that the results (particularly for the butane C–H relaxation) depend somewhat on the time span chosen for the fit. Nevertheless, the computed correlation coefficients for all the least-squares fits are larger than 0.985. In Table IV we compare the relaxation times obtained from a single-exponential fit to the C_6–H vector in heptane with the results from the time integral of the angular correlation function (eq 8). For the complete dynamics (top row of results), the time integral of the correlation function gives a value for the relaxation time about 14% smaller than that estimated from a single-exponential fit. Such a difference is not important for the analysis described below.

The relaxation times listed in Tables II and III demonstrate a number of important trends. They can be summarized: (a) the relaxation times for these small alkanes in water, whose overall tumbling puts them in the motional narrowing limit, are typically between 5 and 50 ps; (b) the relaxation times increase as the chain length increases from butane to heptane; (c) the relaxation times increase from the ends of the heptane chain toward the center; (d) the relaxation of the Y_0^1 correlation functions are always slower than the Y_m^2 but the ratio of $(\tau_{l=1}/\tau_{l=2})$ is less than 3; and (e) the C–H internuclear vectors relax faster than the C–C vectors. Results a, b, and c are in accord with experiment; there are no data concerning d and e.

Heptane is expected to tumble more slowly than butane in solution due to the increased molecular dimensions of the heptane chain. It is of interest to compare the relaxation times calculated from the trajectories with values based on an estimate of the rotational diffusion coefficients for rigidly tumbling alkanes in solution. Viewing the butane molecule as an assembly of four spheres, each centered on a carbon nucleus (the extended atom model), the rotational diffusion coefficient, D_r, for the rigidly tumbling molecule can be estimated from a Stokes–Einstein relationship of the form[46]

$$D_r = kT/\zeta\sum l_i^2 \qquad (19)$$

Table V. Alkane NMR Spin-Lattice Relaxation Times

	T_1, s	$T_1^{C_2}/T_1^{C_i}$
Trajectory Results[a]		
butane carbons		
C2, C3	5.9 ± 0.12	
heptane carbons		
C2, C6	1.94 ± 0.18	
C3, C5	1.82 ± 0.14	1.07
C4	1.75 ± 0.24	1.11
Experimental Results[b]		
heptane carbons		
[C1, C7]	[10.9]	[0.81[c]]
C2, C6	13.2	
C3, C5	12.8	1.03
C4	12.0	1.10
eicosane carbons		
[C1, C20]	[3.6]	[0.43[c]]
C2, C19	2.3	
C3, C18	1.6	1.44
C4, C17	1.1	2.09
interior[d]	0.8	2.88

[a] 25 °C, η = 1 cP, aqueous solution. [b] 39 °C, η = 0.34 cP for neat heptane, ref 10. [c] Normalized to the same number of directly bonded protons. [d] Individual values were not obtained.

where l_i is the distance of the ith sphere from the center of hydrodynamic resistance and ζ is the monomer friction coefficient. The relaxation times for the Y_m^2 are predicted for *rigidly* tumbling trans butane to be 12 ps and for the more compact cis butane to be 10 ps. The relaxation times obtained from the flexible butane trajectories are about a factor of 2 smaller than the estimates based on a rigid tumbling model. This difference is in qualitative accord with the results of recent estimates[47] of the increased rotational mobility of molecules with internal flexibility. A quantitative comparison between the rigid and flexible results requires the complete diffusion tensors for the rigid butane conformers.[48]

With regard to the ratio of relaxation times for the first- and second-order spherical harmonics (Tables II and III), values less than 3 are indicative of deviations from simple diffusive reorientation for rigid spherical molecules; for such systems extended diffusion and finite jump models for the rotational motion have been introduced.[43] Since the alkane trajectories were constructed from a small-step diffusion equation, the deviation from the ratio of 3 must be due to other sources. It could originate from the nonspherical character of the molecules (more than one component to the diffusion tensor), from their flexibility, or from both. Further, as already mentioned, the description of the rotational relaxation in terms of a single exponential is an approximation for these molecules.

The relaxation of the butane and heptane C–H internuclear vectors is of particular interest because these are the coordinates probed by a ^{13}C NMR experiment. Since motions about both C_{i-1}–C_i and C_i–C_{i+1} axes contribute to the relaxation of C_i–H, the relaxation times of the C–H vectors are shorter than the relaxation times of the neighboring carbon–carbon bonds. From the C–H relaxation times listed in Tables II and III, the ^{13}C spin–lattice relaxation times (T_1) are calculated by means of eq 9. Table V lists the predicted ^{13}C T_1's for each of the methylene carbons of butane and heptane; the final column gives the ratio of T_1 for carbon C_2 and the ith internal carbon. Unfortunately, experimental measurements of these relaxation times for small alkanes in *aqueous* solution are not available. However, measurements of T_1's have been reported for neat liquid alkanes[10,11] and some of these results are given in Table V. The NMR relaxation times calculated from the trajectories and from experiment are of the order of seconds. This time scale is characteristic of small

(46) J. Happel and H. Brenner "Low Reynolds Number Hydrodynamics", Prentice Hall, Englewood Cliffs, N.J., 1965.
(47) S. Harvey, *Biopolymers*, **18**, 1081 (1979).
(48) D. C. Knauss, G. T. Evans, and D. M. Grant, *Chem. Phys. Lett.*, **71**, 158 (1980).

molecules tumbling in the motional narrowing limit, in contrast to the millisecond NMR relaxation times commonly observed for macromolecules whose tumbling times are much closer to the reciprocal of the Larmor frequencies of standard spectrometers. Quantitative comparison of the heptane results shows that the T_1's calculated from the trajectories are shorter than the experimental results by a factor of ~6. One source of this difference is in the larger viscosity of the aqueous solution relative to neat liquids. The viscosities of the neat alkanes at the experimental temperature of 40 °C are three to four times smaller than the viscosity used for the aqueous solution calculation (η = 0.27 cP for hexane at 40 °C, η = 0.34 cP for heptane at 40 °C, compared with η = 1 cP for aqueous solution). If we assume the trajectory results scale linearly with the viscosity (as they are expected to do in the diffusive limit), we find that the calculated relaxation times for heptane are a factor of 1.5 to 2 shorter than the experimental values. Differences of this order may be due to the limitations of the stochastic dynamics model;[34] these include the neglect of the inertial term of the complete Langevin equation, the neglect of hydrodynamic interaction, and the use of an atomic friction coefficient obtained from the translational diffusion coefficient of a monomer unit in the Langevin equation for the alkane chain. In this regard, if the covalent radius (0.77 Å) for the carbon atoms instead of the van der Waals radius (1.85 Å) is used to obtain the monomer friction coefficient as has been suggested,[48] the calculated T_1's are increased by 2.4 and are closer to experimental values. It is important to note that, while the absolute values of the predicted T_1's are somewhat too short, the trajectory results reproduce the experimentally observed gradient in T_1's along the heptane chain.

From the experimental values in Table V it can be seen that the T_1 gradient along the alkane chains increases progressively with chain length; i.e., the ratios $T_1^{C_2}/T_1^{C_i}$ (i = 3, 4) are considerably larger in eicosane than in heptane. This is consistent with the idea that the overall tumbling contribution to the relaxation of carbons close to the ends of the n-alkane chains decreases as the size increases;[9-11] that is, if we make use of the empirical relation given in eq 12, τ_0 becomes larger for longer alkanes, while τ_i for the CH bonds near the ends of the chain is much less affected and finally dominates the relaxation ($\tau_{eff} \rightarrow \tau_i$ as τ_0 increases). Lyerla et al.[10] have, in fact, interpreted the ^{13}C T_1's of a series of alkanes by means of eq 12 and obtained consistent results. While detailed trajectory studies for a series of alkanes longer than heptane are required to determine the range of validity of the empirical relation (eq 12), a preliminary analysis is reported below.

c. Test of Simplified Models. To explore whether relaxation in the motional narrowing limit can be divided into contributions from tumbling and segmental motions, the relaxation of the C_6 carbon of heptane was analyzed. The heptane molecule molecular tumbling axis was defined by atoms C_1–C_2–C_3 (see Appendix A). This somewhat arbitrary choice was made because it is appropriate for the analysis of Section IV. Both the tumbling correlation function and the correlation functions describing the internal relaxation were calculated directly from the trajectory. Figure 3 compares the decay of the second-order spherical harmonics of the C_6–H internuclear vector calculated exactly from the trajectory (eq 13) with the relaxation of this vector obtained when correlations between the tumbling and internal motions are broken (eq 14). Also given in the figure are the separate relaxation of the tumbling and the internal motion parts of the correlation function (see caption of Figure 3). The first three correlation functions (Figure 3a–c) decay to zero, but the internal motions part (Figure 3d) does not because there is not enough freedom to sample all solid angles in this short alkane. Further, the decay of the internal motion part is much slower than that of the other functions. The slower internal motion decay, relative to overall tumbling, contrasts with the behavior expected for the longer alkanes, as described above. As to the comparison of Figure 3a–c, all three correlation functions are similar, with the uncoupled function (b) decaying faster and the tumbling part alone (c) slower than the exact correlation function (a). In order to quantitate these comparisons, Table IV lists the time integrals (eq 8) of these correlation functions and the fits to them of single exponentials over several time spans. The results indicate that for this particular carbon and choice of molecular tumbling axis, separating the dynamics into contributions from tumbling and internal relaxation is a rather good approximation. Considering the time integral first, we see that the exact correlation function value of 0.68 is close to that (0.58) obtained from the product of the uncoupled tumbling and internal correlation functions. That the product of the uncoupled correlation functions yields a smaller value than the exact result indicates that correlations between the motions which reorient the molecule and the segmental motions tend to preserve chain orientation. A corresponding comparison of the least-squares fits to the complete and uncoupled correlation functions also shows good agreement. However, the sensitivity of the results to the time period used (see Table IV) does not permit us to say which correlation function has the longer relaxation time.

Further analysis of the applicability of eq 12 requires individual values for τ_0 and τ_i from the stochastic trajectory. A tumbling relaxation time can be obtained directly from the time integral (eq 8) applied to that part of the uncoupled correlation function (i.e., to

$$(4\pi)^{-1}\sum_a \langle \mathbf{D}_{ma}^{2*}(\Omega_0(t))\mathbf{D}_{ma}^{2}(\Omega(0))\rangle \qquad (20)$$

shown in Figure 3c) or alternatively from the corresponding exponential fits. Least-squares fits of the tumbling relaxation to a single exponential are more dependent on the chosen time span than the fit to the complete correlation function; the estimates of the tumbling relaxation time vary from 13 ps from a fit of the first 10 ps to a single exponential to 22 ps when the first 50 ps are included. The time integral of the tumbling relaxation agrees best with a single exponential fit over the first 20 ps; the exponential gives 15.8 ps as compared with the time integral value of 15.2 ps (see Table IV). Since the correlation function describing internal relaxation does not decay to zero (see Figure 3d), the time integral, which goes from t = 0 to ∞, does not provide a definition of the internal relaxation time. An internal relaxation time can still be defined by a fit to a single exponential of the initial rate of decay of the internal motion correlation function; that is, we write

$$\sum_{bb'} \langle \mathbf{D}_{ab}^{2*}(\Omega_i(t))\mathbf{D}_{ab'}^{2}(\Omega_i(0))\rangle \sim (1 - A_\infty)e^{-t/\tau_i} + A_\infty \qquad (21)$$

where A_∞ is the infinite-time plateau value. Alternatively, the time integral could be performed with the plateau value, A_∞, subtracted from the correlation function. This provides a satisfactory definition of an internal relaxation time, τ_i, when the tumbling time, τ_0, is shorter than or equal to the internal relaxation time τ_i. With estimates of the tumbling and internal relaxation times from Table IV (τ_0 = 16 ps and τ_i = 39 ps), the empirical relation (eq 12) yields an estimate for the total relaxation time of τ_{eff} = 11 ps, as compared with the value of τ_{eff} = 10 ps obtained from a fit of the exact dynamics to a single exponential. Thus, the present trajectory results support the usefulness of the empirical relation, eq 12. A more detailed analysis for longer hydrocarbons is in progress with particular attention focused on the definition of the molecular tumbling coordinate system, which should be related to the slowest relaxing modes of the alkane chain.

In uncoupling the tumbling and internal motions, it is possible to examine the introduction of an additional approximation (see Figures 3e and 3f). The evaluation of the correlation function involves a double summation over a and a' (eq 14a) because the off-diagonal contributions to the tumbling correlation function, $\langle \mathbf{D}_{ma}^{2*}(\Omega_0(t))\mathbf{D}_{ma'}^{2}(\Omega_0(0))\rangle$, are not in general zero for a flexible molecule of arbitrary shape. For an asymmetric rigid rotor these correlation functions can be expanded in terms of the symmetric rotor eigenfunctions;[43] they are zero initially, become nonzero at some later time, and finally decay to zero again. For the flexible heptane chain, this behavior is observed for the off-diagonal terms (Figure 3f). However, their numerical value is very small at all times and the relaxation is accounted for almost entirely by in-

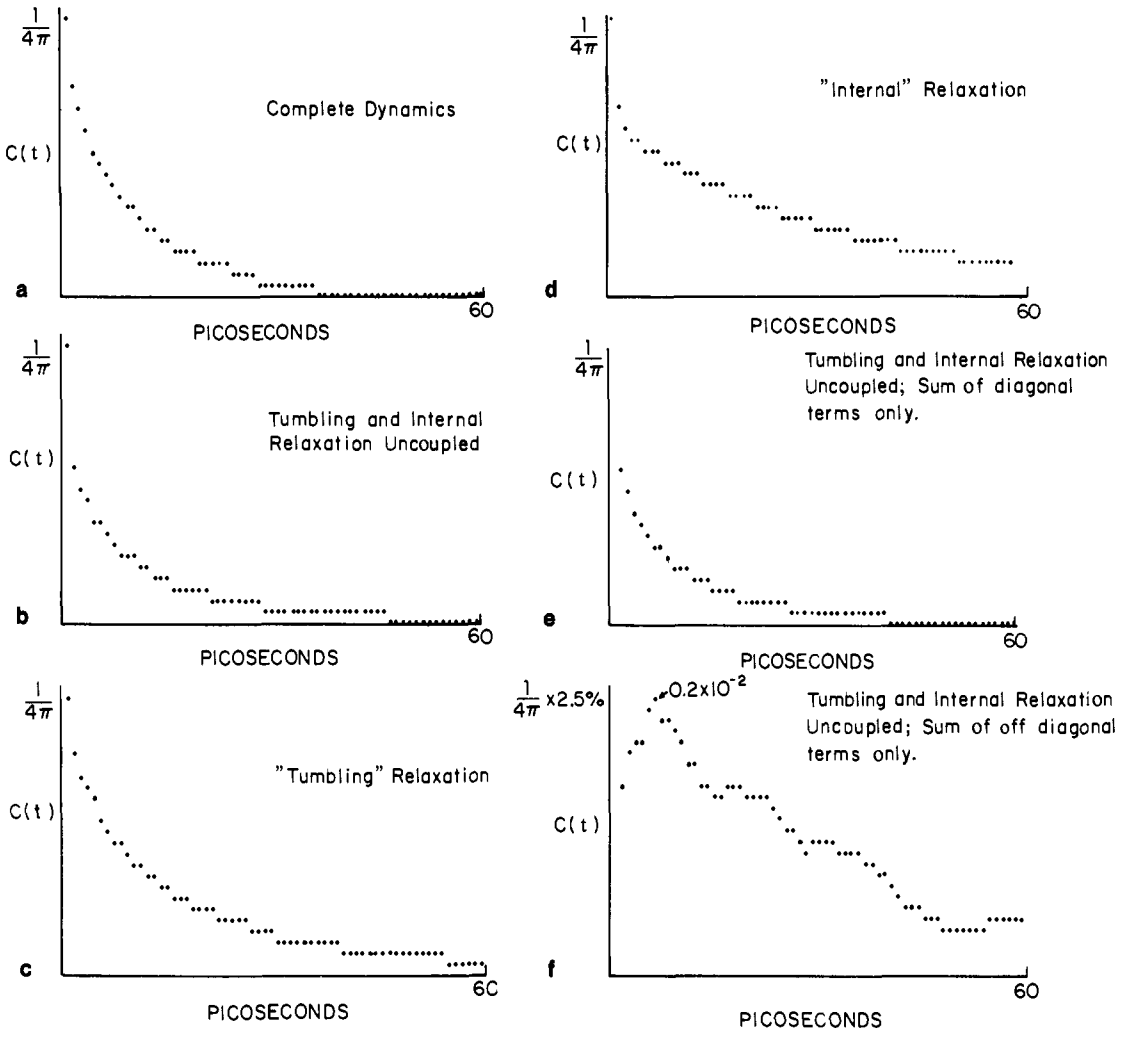

Figure 3. Relaxation of the second-order spherical harmonics $\langle Y_0^2(\theta(t)\phi(t))Y_0^2(\theta(0)\phi(0))\rangle$ of the C_6–H internuclear vector calculated from the heptane trajectory: (a) exact results from trajectory (eq 13); (b) results when correlations between tumbling and internal motions are broken (eq 14a); (c) relaxation of diagonal tumbling correlation function, $(1/4\pi)\sum_a \langle \mathbf{D}_{ma}^{*2}(\Omega_0(t))\mathbf{D}_{ma}^2(\Omega(0))\rangle$ in eq 14a; (d) relaxation of internal correlation function, $^1/_5\sum_{abb'}\langle \mathbf{D}_{ab}^{2*}(\Omega_i(t))\mathbf{D}_{ab'}^2(\Omega_i(0))\rangle Y_b^2(\theta_{mol},\phi_{mol})Y_{b'}^{2*}(\theta_{mol},\phi_{mol})$, in eq 14a; (e) sum over diagonal terms ($a = a'$) in eq 14a; and (f) sum over off-diagonal terms ($a \neq a'$) in eq 14a.

cluding only the diagonal terms ($a = a'$) in the sum of eq 14; the accuracy of this approximation can be determined by comparing Figures 3b and 3e, which are seen to be essentially identical. The diagonal approximation reduces to eq 14b if an isotropic tumbling model is appropriate. Otherwise, the three principal components of the diffusion tensor for the tumbling motion have to be introduced.[24,26]

IV. NMR Relaxation of a Side Chain Attached to a Tumbling Macromolecule

In this section, the heptane trajectory is used as outlined in Section II to evaluate T_1, T_2, and NOE for a model aliphatic side chain with four internal rotational angles protruding from a tumbling macrmolecule. By employing the Wigner matrices to describe the relaxation of the heptane C–H internuclear vectors with respect to a coordinate frame embedded in the alkane (eq 14 and Figure 1), we are able to superimpose arbitrary molecular tumbling on the internal chain relaxation. Coupling between macromolecular tumbling and side chain motion is not considered; this is a good approximation since side chain motion has a very small effect on the dimensions of macromolecules and the size of proteins.[50]

For macromolecules tumbling with relaxation times close to or slower than the Larmor frequency, the ^{13}C NMR relaxation parameters have a qualitatively different behavior from what is observed in the motional narrowing limit (Section III). Since there is now significant spectral density at the Larmor frequency, the complete expressions (eq 2–4) have to be used. One effect is that the NMR parameters are dependent on the strength of the applied magnetic field. Also, the spin–spin relaxation time, T_2, given in eq 3, has a contribution from the integral of the angular correlation function, $J(0)$, and can be much shorter than the spin–lattice relaxation time, T_1. For side chain carbons protruding from a slowly tumbling macromolecule the extra flexibility can have widely varying effects on the observed NMR relaxation. For a molecule tumbling more slowly than the Larmor frequency, the internal motions can decrease the NMR relaxation times. Alternatively, the effect of internal motions with a large angular range and high frequency can be to average out the tumbling contribution to the spectral density and increase the observed relaxation time. The reorientation of longer side chains involves several rotational axes and the motions about these axes have a cumulative effect; i.e., rotation about a particular axis reorients all atoms further out along the chain. Thus, it is possible for the various carbons along such a chain to show significantly different relaxation behavior.

The side chain internal dynamics has been shown[34] to separate into two very different time scales. The shorter, on the order of tenths of picoseconds, corresponds to torsional fluctuations within a potential well, and the longer, on the order of one to two hundred picoseconds, corresponds to transitions between minima of the potential (Figure 4). The internal dynamics is found to be such that the short-time oscillations within a well are expected to have only a small effect on the NMR relaxation rates; they are expected to be dominated by the longer time transitions between wells that lead to larger magnitude reorientations of the C–H internuclear

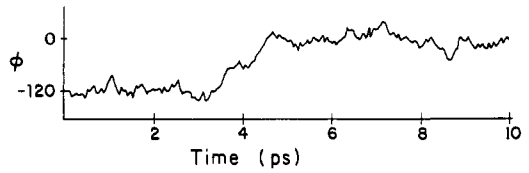

Figure 4. A 10-ps segment of a trajectory showing one isomerization from gauche (−) to trans states and the subpicosecond, small amplitude oscillations (jitter) within the gauche and trans wells.

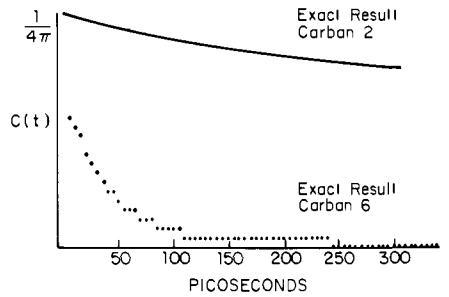

Figure 5. Comparison of relaxation of angular correlation function for C_6–H, the vector furthest out along the side chain (eq 16), with the result for C_2–H, the vector tumbling rigidly with the macromolecule; the tumbling time is τ_0 = 1 ns.

vectors. Consequently, the analytic "independent lattice jump model", introduced in Section II, is a natural first choice to describe the internal dynamics from the viewpoint of its contribution to the NMR relaxation parameters. Thus, in addition to using the trajectory for a complete evaluation of the side chain relaxation, we provide a detailed comparison with the results of the lattice jump model. Within the context of side chain motions similar to the alkane internal dynamics, and for the choice of macromolecular tumbling times and field strengths we have investigated, the present test of the applicability of the lattice jump model serves to delineate its utility for interpreting NMR data for macromolecules.

a. Exact Trajectory Results. The NMR relaxation parameters T_1, T_2, and NOE for each of the carbons (C_2 through C_6) calculated exactly by means of eq 14a and 16 from the trajectory are listed in Table VI. Results obtained for three isotropic molecular tumbling times (τ_0 = 1, 10, and 100 ns) and for two spectrometer frequencies (15 and 68 MHz) are compared. The shorter tumbling time (τ_0 = 1 ns) is appropriate for small proteins such as PTI, τ_0 = 10 ns is applicable to proteins the size of myoglobin, while the long tumbling time (τ_0 = 100 ns) is appropriate for relaxation in lipid micelles. The ^{13}C Larmor frequencies 15 and 68 MHz correspond to typical low- and high-field spectrometers.

It is apparent from Table VI that there is an important variation in the results depending on the system (value of τ_0) and on the experimental conditions (value of ω). For the case of dipolar relaxation, the NMR relaxation times T_1 and T_2 tend in general to increase with spectrometer frequency, as can be seen by comparing the results at 15 and 68 MHz. Further, for a given system and set of conditions, there is a large gradient in T_1, T_2, and NOE values along the chain; e.g., T_1 and T_2 can range from less than 10 ms for a C_2 carbon tumbling rigidly with the macromolecule

Table VI. Side Chain NMR Parameters, Exact Result

	15 MHz			68 MHz		
	T_1, ms	T_2, ms	NOE $(1+\eta)$	T_1, ms	T_2, ms	NOE $(1+\eta)$
			τ_0 = 1 ns			
C_2 (analytic)	26.5	25.8	2.80	58.3	48.9	1.70
C_3	112	110	2.86	179	163	2.34
C_4	290	290	2.97	312	308	2.90
C_5	452	450	2.96	493	486	2.90
C_6	627	625	2.97	682	672	2.90
			τ_0 = 10 ns			
C_2 (analytic)	11.9	7.3	1.30	133	11	1.16
C_3	60	40	1.63	230	57	2.44
C_4	243	223	2.74	292	247	2.91
C_5	368	313	2.50	492	358	2.95
C_6	519	454	2.60	665	515	2.92
			τ_0 = 100 ns			
C_2 (analytic)	62.4	1.2	1.16	1,270	1.2	1.15
C_3	171	7.1	2.18	302	7.2	2.87
C_4	274	101	2.93	293	103	2.93
C_5	466	99	2.86	496	100	2.94
C_6	617	163	2.89	667	165	2.94

to greater than 500 ms for the most mobile C_6 carbon, while the NOE varies from its minimum to its maximum possible value.

Of the many comparisons that can be made with the results in Table VI, we consider first the calculations for 15 MHz, τ_0 = 1 ns where the NMR relaxation parameters are characteristic of the motional narrowing limit; i.e., T_1 equals T_2 for all of the carbons along the chain and the NOE value is almost maximal, even for the slowest relaxing carbon. The NMR relaxation times for this case are inversely proportional to the time integrals of the angular correlation functions (eq 8–10). Figure 5 compares the angular correlations for the C_2 and C_6 carbons. The much more rapid decay for the C_6–H vector results in a 25-fold increase in the value of T_1 over that for the C_2 carbon; i.e., the fast reorientation of the C_6–H vector averages out the effect of the macromolecular tumbling, which is in the frequency range to produce highly efficient relaxation (as found for C_2). Thus, the internal flexibility has a dramatic effect on the NMR relaxation. This is to be contrasted with the results for the heptane chain in solution. For that system, which is also in the motional narrowing limit, the much higher tumbling rate (on the same order as the internal motions) leads to longer relaxation times and a much weaker variation of T_1 with position in the chain. It is of interest in the macromolecule that the T_1 values of C_6 with its large internal motion freedom approach that obtained for the free heptane.

For the short tumbling time (τ_0 = 1 ns) at the higher frequency (68 MHz), the inner carbons (C_2 and C_3), whose motion is dominated by the overall tumbling, are beginning to show a deviation from motional narrowing behavior (i.e., $T_1 \neq T_2$ and the NOE value is less than maximum). The outermost carbons, particularly C_6, remain in the motional narrowing limit for this case. For the longer tumbling times (τ_0 = 10 and 100 ns), there are significant deviations from the motional narrowing limit for all carbons at both spectrometer frequencies. Even for C_6 where

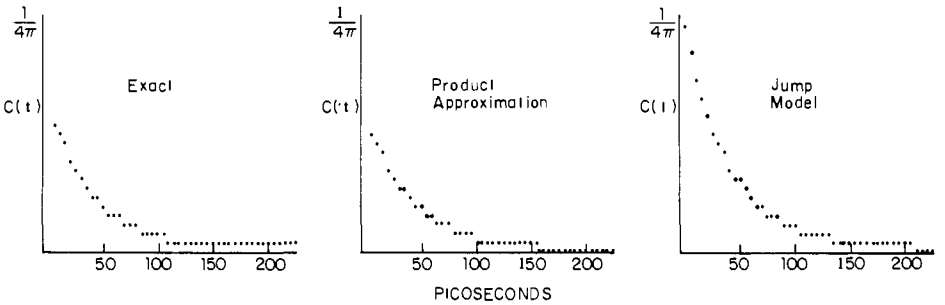

Figure 6. Comparison of the C_6–H angular correlation function: (a) calculated exactly from the trajectory (eq 13); (b) calculated from the product approximation (eq 17); and (c) calculated from the independent lattice jump model (eq 18).

Table VII. Side Chain NMR Parameters, Product Approximation

	15 MHz			68 MHz		
	T_1, ms	T_2, ms	NOE $(1+\eta)$	T_1, ms	T_2, ms	NOE $(1+\eta)$
			τ_0 = 1 ns			
C_2 (analytic)	26.5	25.8	2.80	58.3	48.9	1.70
C_3	112	110	2.86	179	163	2.34
C_4	292	291	2.97	319	314	2.88
C_5	497	496	2.98	520	516	2.93
C_6	841	840	2.98	856	853	2.97
			τ_0 = 10 ns			
C_2 (analytic)	11.9	7.3	1.30	133	11	1.16
C_3	60	40	1.63	230	57	2.44
C_4	238	214	2.67	300	242	2.89
C_5	439	413	2.82	493	441	2.94
C_6	787	769	2.92	823	790	2.97
			τ_0 = 100 ns			
C_2 (analytic)	62.4	1.2	1.16	1,270	1.2	1.15
C_3	171	7.1	2.18	302	7.2	2.87
C_4	278	86	2.91	302	88	2.94
C_5	475	224	2.95	495	227	2.96
C_6	809	578	2.98	822	583	2.98

the T_1 and NOE behavior approach the motional narrowing limit, the T_2 values are generally significantly shorter than T_1 due to the presence of a nonnegligible $J(0)$ contribution.

At 15 MHz and τ_0 = 1 ns, the spin–lattice relaxation time (T_1) for the rigidly tumbling carbon C_2 is 26.5 ms, while for τ_0 = 10 ns, T_1 is 11.9 ms. However, at 68 MHz T_1 increases from 58.3 to 133 ms as the tumbling time increases. The reason for this difference in the behavior of T_1 is that at 15 MHz the slowly tumbling molecule is more efficient at relaxing the C_2 carbon, whereas at 68 MHz the more rapidly tumbling molecule is more efficient. This behavior is not found for the T_2 relaxation; because of the presence of a zero-frequency component, relaxation is more effective at a longer tumbling correlation time, independent of spectrometer frequency.

To examine the contributions of internal motions to the relaxation, we compare the high-field (68 MHz) results at the two slower tumbling times (10 and 100 ns). For the rigid carbon C_2, the macromolecule is tumbling too slowly for efficient relaxation; consequently, $T_2 \ll T_1$ and the NOE value is minimal. Side chain flexibility can enhance relaxation rates due to the presence of additional frequency components closer to the Larmor frequency. This does not occur for the side chain tumbling at τ_0 = 10 ns, where the increase in T_1 along the chain is monotonic. However, the micelle tumbling (100 ns) is so slow with respect to the Larmor frequency that internal motions do increase the relaxation rates. The rigid C_2 carbon T_1 is longer than 1 s while C_3, which can reorient about one side chain rotation axis, has a T_1 of only 302 ms. The high-field T_1 and T_2 values for C_6 furthest out along the chain demonstrate that T_1 is sensitive to the high-frequency molecular motions, whereas T_2 probes primarily the low-frequency motions. For C_6, T_1 at τ_0 = 10 ns and at 100 ns are almost identical (665 and 667 ms, respectively). By contrast, T_2 is much shorter for the longer tumbling time (for C_6, T_2 = 515 ms at τ_0 = 10 ns and T_2 = 165 ms at τ_0 = 100 ns). This result demonstrates the importance of measuring both T_1 and T_2 in order to obtain information about molecular dynamics from NMR.

b. Simplified Models. We now evaluate the NMR parameters obtained from simplified models for the side chain dynamics and compare the results obtained from these models with the exact results. In the product approximation (eq 17), motions about the four side chain rotational axes are assumed to be uncorrelated. The NMR parameters calculated in the product approximation are presented in Table VII. That the T_1, T_2, and NOE values for carbons C_2 and C_3 are identical in Tables VI and VII is due to the fact that the C_2 carbon is tumbling rigidly with the macromolecule and the C_3 carbon is reorienting about only one axis, so that no additional approximation is introduced for these two carbons. For the other carbons, the calculated relaxation times are always *longer* in the product approximation in comparison with the exact results. This is expected since correlations in the motions about the successive axes decrease the rate at which the tumbling relaxation is averaged by the internal motions. For most of the cases studied, the NMR parameters calculated from the product approximation are close to the exact results. For carbon 4 the results calculated in the product approximation are within 5% of the exact values. Proceeding out along the chain, the agreement between the two sets gets worse, but even for carbon 6 the approximate NMR parameters are within a factor of 2 of the exact results. An exception to this general agreement is found in the high-field T_2 values for micellar tumbling (τ_0 = 100 ns); the exact result is T_2 = 165 ms for C_6 whereas in the product approximation T_2 = 583 ms. This large discrepancy is due to the fact that the product approximation does not properly describe the long time values of the correlation functions determined from the internal motions of the chain (see below). That the product approximation generally gives good results suggests that correlations among neighboring dihedral angles do not play a significant role in the chain isomerization dynamics. This is attributed in part to the sizable energy barrier involved in alkane trans-gauche isomerization;[49] the activation energy barrier for two simultaneous isomerizations is sufficiently high that they make only a small contribution to the relaxation.

Table VIII. Heptane Isomerization Rate Constants[a]

rotational angle	K_T ($\times 10^{-9}$ s^{-1})	K_G ($\times 10^{-9}$ s^{-1})
ϕ_1	3.05	7.4
ϕ_2	2.60	4.8
ϕ_3	2.05	4.1
ϕ_4	3.35	6.5

[a] Trajectory results taken from ref 34.

Table IX. Side Chain NMR Parameters, Lattice Jump Model

	15 MHz			68 MHz		
	T_1, ms	T_2, ms	NOE $(1+\eta)$	T_1, ms	T_2, ms	NOE $(1+\eta)$
			τ_0 = 1 ns			
C_2 (analytic)	26.5	25.8	2.80	58.3	48.9	1.70
C_3	99	97	2.86	162	147	2.31
C_4	226	225	2.96	252	247	2.85
C_5	339	339	2.98	358	355	2.92
C_6	511	510	2.98	520	518	2.97
			τ_0 = 10 ns			
C_2 (analytic)	11.9	7.3	1.30	133	11	1.16
C_3	52	35	1.59	216	50	2.40
C_4	179	158	2.63	235	183	2.85
C_5	296	278	2.81	338	301	2.92
C_6	477	469	2.94	496	481	2.96
			τ_0 = 100 ns			
C_2 (analytic)	62.4	1.2	1.7	1,270	1.2	1.15
C_3	159	6.0	2.11	295	6.1	2.88
C_4	219	60	2.90	241	61	2.91
C_5	324	151	2.94	339	153	2.95
C_6	437	377	2.98	496	380	2.98

The independent lattice jump model idealizes the chain dynamics to instantaneous jumps among stable side chain configurations; the details of the model are given in Appendix B. Between jumps the side chain is assumed to be tumbling rigidly with the macromolecule. NMR parameters were calculated from the independent lattice jump model (eq 18 and Appendix B) with the isomerization parameters obtained from the heptane stochastic trajectory; the rate constants K_G and K_T are given in Table VIII, which is taken from ref 34. The values for T_1, T_2, and NOE obtained are listed in Table IX; for C_2, which moves rigidly with the macromolecule, the values are identical with those in Tables VI and VII. In contrast to the product approximation, which yields T_1 and T_2 values that are uniformly longer than the exact results, those calculated from the jump model are uniformly shorter than

(49) M. R. Pear, S. H. Northrup, J. A. McCammon, M. Karplus, and R. M. Levy, *Biopolymers*, **20**, 629 (1981).

the exact results. For carbon 3, the jump model values are within 10% of the exact results; e.g., for $\tau_0 = 1$ ns and 15 MHz the exact value is $T_1 = 112$ ms as compared with $T_1 = 99$ ms from the model; corresponding agreement is obtained for all τ_0 values and spectrometer frequencies. For carbons further out along the chain, the jump model relaxation times differ more from the exact values; they are generally within 30% although the high-field T_2 values for micellar tumbling ($\tau_0 = 100$ ns) differ by 50% for carbon 6. An important source of error introduced by the jump model is readily apparent when plots of the angular correlation functions are examined. Figure 6 compares the relaxation of the C_6–H angular correlation function calculated exactly from the trajectory (a), calculated from the product approximation (b), and calculated from the jump model (c). The plots of the product approximation and the exact relaxation are very similar with a slightly faster decay obtained from the product approximation, as expected. The jump model, however, exhibits a considerably slower initial decay as compared with the two other functions. It is this slower decay which limits the fast time averaging of the C_6–H dipole vector and leads to more efficient relaxation. The reason for the absence of the fast initial decay in the jump model is that it does not include the high-frequency, small-amplitude oscillations that occur within a given potential well. This deficiency of the jump model is well-known and can be improved in "jitter plus jump" relaxation models.[51,52] The very good results obtained from the pure independent lattice jump model in the present case are due to a cancellation of errors. The model leaves out the small amplitude oscillations of the chain (Figure 4) and it uncouples the jumps of the different dihedral angles from one rotational minimum to another. Uncoupling the correlation in the motions along the chain leads to a more rapid decay (less efficient NMR relaxation), while ignoring the short time oscillations of the chain leads to a slower decay (more efficient NMR relaxation). Although these corrections are not very large for the present system and conditions (e.g., compare Tables VII and VIII), the fact that they have opposing effects and are neglected simultaneously means that the jump model NMR relaxation times are near the exact values and generally somewhat closer than the product model results. However, it should be remembered that there are likely to be cases (e.g., in the interior of proteins) where jumps are so rare that the oscillations within a well make a much more important contribution to the relaxation. Their neglect, as in the simple jump model, would then no longer be a good approximation and alternative simple models (e.g., the restricted diffusion model[26,27]) would then be likely to yield more satisfactory results.

c. Long-Time Behavior of Correlation Functions. We conclude this section with a discussion of the problems incurred by the models at long times. The angular correlation functions describing the internal chain dynamics have the long-time (equilibrium) behavior given by the equation

$$\langle \sum_{bb'} \mathbf{D}_{ab}^{*2}(\Omega_i(t))\mathbf{D}_{ab'}^{2}(\Omega_i(0))\rangle_{t\to\infty} = |\langle \sum_{b} \mathbf{D}_{ab}^{2}(\Omega_i(0))\rangle|^2 \qquad (22)$$

that is, for times long compared to the characteristic decay time of the correlation function, the value reduces to the ensemble average of the equal time result.[43] Substituting eq 22 into eq 14b, we see that the time correlation functions used to calculate the NMR relaxation parameters are determined at long times by the value of the Wigner functions averaged over the equilibrium distribution of chain configurations. For certain systems these long-time contributions are very important (e.g., slowly tumbling vesicles, nonisotropic systems such as membranes, and liquid crystals). Both the product approximation and the independent jump model do not average the chain configurations correctly, so that the wrong long time values of the angular correlation functions are obtained. The magnitude of the differences is shown in Table X, which compares the configurational averages of the Wigner functions obtained from the trajectory with the product and independent lattice jump approximations. The exact results show a pattern of oscillations superimposed on an overall decay with distance along the chain; analogous behavior is obtained in the rotational isomeric state model.[53] No such oscillations appear in either the product or lattice jump models. Further, Table X shows clearly that the averages in both approximate models are diverging from the exact results along the chain. For carbon 6, the configurational average of the Wigner functions calculated exactly is almost a factor of 10 larger than the results from either approximation. This suggests conditions under which neither the product nor the independent lattice jump model can provide an adequate description of the relaxation. Errors in the configurational averaging become more important as the separation in the time scales of the internal motions and the tumbling increases. For the cases considered here, the consequences of errors in configurational averaging are most apparent for the high-field T_2 values obtained with the longest tumbling time ($\tau_0 = 100$ ns). For this case, T_2 calculated from the simplified models is two to four times longer than the exact T_2 values.

Table X. Configurational Average of Wigner Functions[a]

carbon	exact	product approx	independent lattice jump model
C_3	0.126×10^{-1}	0.126×10^{-1}	0.148×10^{-1}
C_4	0.580×10^{-3}	0.740×10^{-3}	0.112×10^{-2}
C_5	0.740×10^{-3}	0.220×10^{-3}	0.340×10^{-3}
C_6	0.420×10^{-3}	0.460×10^{-4}	0.560×10^{-4}

[a] Configurational average of $\Sigma_a[0.2][(|\Sigma_i D_{ai}^{*2}(\Omega)Y_i^2(\theta,\phi)|)^2$ from eq 14b and 22.

V. Conclusions

Stochastic dynamics trajectories for alkanes in aqueous solution have been used to examine a variety of problems that arise in the interpretation of carbon-13 NMR relaxation experiments. Exact results for T_1, T_2, and NOE values obtained from these trajectories have been employed to analyze the relaxation behavior of small alkanes and macromolecular side chains and to test the validity of simplified relaxation models for these systems. The NMR relaxation of small flexible molecules was studied in the motional narrowing limit. Results were obtained for the spin–lattice relaxation times of butane and heptane in aqueous solution. A gradient in relaxation times along the heptane chain was found that is in agreement with the measured values for the neat liquid. The empirical separation of the relaxation contributions in these molecules into a tumbling plus an internal motion term was shown to yield useful results. In order to confirm the present results, it would be helpful to have available stochastic dynamic calculations for longer chains and experimental measurements of NMR relaxation times for alkanes dissolved in more viscous liquids.

By using the Wigner functions to describe the heptane relaxation with respect to a coordinate frame embedded in the molecule, we have been able to analyze models for side chain relaxation in macromolecules. Uncoupling the motion of the side chain with respect to the internal rotation axes (product approximation) and the jump model incorrectly describe the short-time and long-time relaxation. However, for macromolecules with short alkane-like side chains moving freely in aqueous solvent, both models provide a satisfactory description of the NMR relaxation.

In summary, the present work provides a firm theoretical foundation for the continuing effort to use NMR measurements for the experimental analysis of the dynamics of molecules with internal degrees of freedom.

Acknowledgment. We thank A. Szabo for comments on a preliminary version of the manuscript and J. A. McCammon for helpful suggestions.

Appendix A

To describe the relative contributions of segmental and tumbling motions to the relaxation of a particular carbon–hydrogen vector, we use the Wigner rotation matrices, $D_{ab}^2(\Omega)$, which transform

(50) W. F. Van Gunsteren and M. Karplus, *Biochemistry*, in press.
(51) D. Edholm and C. Blomberg, *Chem. Phys.*, **42**, 449 (1979).
(52) M. Elwenspoek, *Mol. Phys.*, **37**, 689 (1979).
(53) A. Baram and W. M. Gelbart, *J. Chem. Phys.*, **66**, 617 (1977).

the spherical harmonics between coordinate frames related by the Euler angles Ω.[44] We treat the C_6–H vector (Figure 1) as an example. Its relaxation can be described by the motion of five successive coordinate frames, starting with the molecular diffusion axis centered on C_2 and proceeding stepwise along the chain; this is expressed by successive coordinate transformations of axes centered on C_3 through C_6. As indicated in Figure 1, the z axis of the frame centered on C_i is directed along the C_{i-1}–C_i carbon bond; the y axis is perpendicular to the plane formed by the C_{i-1}–C_i and C_i–C_{i+1} bonds; and the x axis is defined so as to complete a right-handed coordinate system; that is,

$$\hat{Z}_i = \frac{\vec{\mathbf{R}}_i - \vec{\mathbf{R}}_{i-1}}{|\vec{\mathbf{R}}_i - \vec{\mathbf{R}}_{i-1}|} \qquad \hat{Y}_i = \frac{\hat{\mathbf{Z}}_i \times \hat{\mathbf{Z}}_{i+1}}{|\hat{\mathbf{Z}}_i \times \hat{\mathbf{Z}}_{i+1}|} \qquad \hat{\mathbf{X}}_i = \hat{\mathbf{Y}}_i \times \hat{\mathbf{Z}}_i \quad \text{(A1)}$$

The molecular diffusion coordinate system (Figure 1, x_D, y_D, z_D) has its z axis pointing along the C_1–C_2 bond and its y axis perpendicular to the plane formed by atoms C_1–C_2–C_3. With this choice of coordinate systems we may evaluate the second-order spherical harmonics defined by the polar angles of the C_6–H vector with respect to the laboratory frame,

$$Y_m^2(\theta,\phi) = \sum_{abcde} D_{ma}^{2*}(\Omega_{LD}) D_{ab}^{2*}(\Omega_{D3}) D_{bc}^{2*}(\Omega_{34}) D_{cd}^{2*}(\Omega_{45}) D_{de}^{2*}(\Omega_{56}) \times Y_e^2(\theta_{mol},\phi_{mol}) \quad \text{(A2)}$$

For the overall rotation we have the Wigner rotation matrix,

$$\mathbf{D}_{ma}^{2*}(\Omega_{LD}) = e^{+im\alpha_0} d_{ma}^2(\beta_0) e^{+ia\gamma_0} \quad \text{(A3)}$$

with $\Omega_{LD} = (\alpha_0, \beta_0, \gamma_0)$ being the Euler angles to transform *from* the laboratory frame *to* the molecular diffusion frame. The Wigner rotation matrices for the internal rotations are

$$\begin{aligned}
\mathbf{D}_{ab}^{2*}(\Omega_{D3}) &= \mathbf{D}_{ab}^{2*}(0,\beta,\phi_1 + \pi) = d_{ab}^2(\beta) e^{+ib(\phi_1+\pi)} \\
\mathbf{D}_{bc}^{2*}(\Omega_{34}) &= \mathbf{D}_{bc}^{2*}(0,\beta,\phi_2 + \pi) = d_{bc}^2(\beta) e^{+ic(\phi_2+\pi)} \\
\mathbf{D}_{cd}^{2*}(\Omega_{45}) &= \mathbf{D}_{cd}^{2*}(0,\beta,\phi_3 + \pi) = d_{cd}^2(\beta) e^{+id(\phi_3+\pi)} \quad \text{(A4)} \\
\mathbf{D}_{de}^{2*}(\Omega_{56}) &= \mathbf{D}_{de}^{2*}(0,\beta,\phi_4 + \pi) = d_{de}^2(\beta) e^{+ie(\phi_4+\pi)}
\end{aligned}$$

Here β is the complement of the C–C–C valence angle (assumed fixed), and ϕ_i is the ith time-dependent rotational angle (see Figure 1). Since we use the polymer convention $\phi_{trans} = 0$ (instead of the peptide convention $\phi_{cis} = 0$), the third Euler angle to transform from coordinates based on C_i to coordinates based on C_{i+1} is $(\phi_i + \pi)$. The $d_{ab}^2(\beta)$ are the real reduced Wigner matrix elements.[44] Finally, θ_{mol} and ϕ_{mol} are the time-independent, spherical-polar coordinates of the C_6–H vector in the local coordinate frame centered on C_6.

We can now use the coordinate transformation properties of the spherical harmonics to examine the contribution of segmental motion to the relaxation of carbon 6. The time correlation function required to evaluate the NMR relaxation parameters for C_6 can be written by use of eq 16 and eq A2–A4 in the form of eq A5.

$$\begin{aligned}
\langle Y_m^2(\theta(t)\phi(t)) Y_m^{2*}(\theta(0)\phi(0))\rangle = \sum_{\substack{abcde \\ a'b'c'd'e'}} \langle [\mathbf{D}_{ma}^{2*}(\alpha_0(t)\beta_0(t)\gamma_0(t)) \mathbf{D}_{ma'}^2(\alpha_0(0)\beta_0(0)\gamma_0(0))] \times \\
[d_{ab}^2(\beta) d_{a'b'}^2(\beta) e^{i[b(\phi_1(t)+\pi)-b'(\phi_1(0)+\pi)]}] [d_{bc}^2(\beta) d_{b'c'}^2(\beta) \times \\
e^{i[c(\phi_2(t)+\pi)-c'(\phi_2(0)+\pi)]}] [d_{cd}^2(\beta) d_{c'd'}^2(\beta) e^{i[d(\phi_3(t)+\pi)-d'(\phi_3(0)+\pi)]} \times \\
[d_{de}^2(\beta) d_{d'e'}^2(\beta) e^{i[e(\phi_4(t)+\pi)-e'(\phi_4(0)+\pi)]} \times \\
Y_e^2(\theta_{mol},\phi_{mol}) Y_{e'}^{2*}(\theta_{mol},\phi_{mol})\rangle \quad \text{(A5)}
\end{aligned}$$

Equation A5 is exact and the time correlation function can be calculated directly from the alkane trajectories by evaluating the time evolution of the spherical polar coordinates of the C_6–H internuclear vector with respect to the laboratory frame, or by employing the successive coordinate transformations given on the right-hand side of eq A5. For 6 ns of the heptane trajectory (1 record/ps) direct evaluation of the correlation function on the left-hand side of eq A5 required 15 s of IBM 360/91 CPU time, while evaluation of the right-hand side of eq A5 by summing over all the terms involved required 29 min.

Analysis of the relaxation of carbon 6 in terms of a tumbling frame centered on C_1 that is uncoupled from the motion of the rest of the chain corresponds to the approximation given in eq 14a. Introduction of the corresponding approximation into eq A5 yields

$$\begin{aligned}
\langle Y_m^2(\theta(t)\phi(t)) Y_m^{2*}(\theta(0)\phi(0))\rangle \simeq \sum_{aa'} \langle \mathbf{D}_{ma}^{2*}(\alpha_0(t)\beta_0(t)\gamma_0(t)) \mathbf{D}_{ma'}^2(\alpha_0(0)\beta_0(0)\gamma_0(0))\rangle \times \\
[\langle \sum d_{ab}^2(\beta) d_{a'b}^2(\beta) e^{i[b(\phi_1(t)+\pi)-b'(\phi_1(0)+\pi)]} \cdots \times \\
d_{de}^2(\beta) d_{d'e'}^2(\beta) e^{i[e(\phi_4(t)+\pi)-e'(\phi_4(0)+\pi)]}\rangle \times \\
Y_e^2(\theta_{mol},\phi_{mol}) Y_{e'}^{2*}(\theta_{mol},\phi_{mol})] \quad \text{(A6)}
\end{aligned}$$

In Section III, we compare eq A6 and A5 for heptane relaxation in the motional narrowing limit. In Section IV we use eq A6 and the heptane trajectory to represent the motion of a side chain protruding from a slowly tumbling macromolecule by assuming that the isotropic tumbling is uncorrelated with the side chain motion. With the orthogonality properties of the $\mathbf{D}_{ma}^J$ matrices and the properties of the isotropic diffusion equation, the time correlation function for isotropic macromolecular tumbling can be written[24,26]

$$\langle \mathbf{D}_{ma}^{J*}(\alpha_0(t)\beta_0(t)\gamma_0(t)) \mathbf{D}_{ma'}^J(\alpha_0(0)\beta_0(0)\gamma_0(0))\rangle = \frac{1}{2J+1} \delta_{aa'} e^{-J(J+1)Dt} \quad \text{(A7)}$$

where D is the diffusion coefficient for the macromolecule. By introduction of eq A7, the relationship for the side chain relaxation (eq A6) reduces to

$$\begin{aligned}
\langle Y_m^2(\theta(t)\phi(t)) Y_m^{2*}(\theta(0)\phi(0))\rangle \approx \frac{e^{-t/\tau_0}}{5} \langle \sum_{\substack{abcde \\ a'b'c'd'e'}} [d_{ab}^2(\beta) d_{ab'}^2(\beta) e^{i[b(\phi(t)+\pi)-b'(\phi(0)+\pi)]}] \cdots \times \\
[d_{de}^2(\beta) d_{d'e'}^2(\beta) e^{i[e(\phi_4(t)+\pi)-e'(\phi_4(0)+\pi)]}] \times \\
Y_e^2(\theta_{mol},\phi_{mol}) Y_{e'}^{2*}(\theta_{mol},\phi_{mol}) \quad \text{(A8)}
\end{aligned}$$

where τ_0 is the macromolecular relaxation time [$\tau_0 = 1/6D$] corresponding to the second rank Wigner matrices. In Section IV, eq A8 is referred to as "exact" in the sense that any correlations in the internal motions of the side chain are explicitly included. Equation A8 can be simplified, as it has been in small-step diffusion and jump models, by assuming that the internal motions are uncoupled as in eq 17. With this assumption, the time correlation function for C_6–H becomes

$$\begin{aligned}
\langle Y_0^2(\theta(t)\phi(t)) Y_0^{2*}(\theta(0)\phi(0))\rangle = \frac{e^{-t/\tau_0}}{5} \sum_{\substack{abcde \\ b'c'd'e'}} d_{ab}^2(\beta) d_{ab'}^2(\beta) d_{bc}^2(\beta) d_{b'c'}^2(\beta) d_{cd}^2(\beta) d_{c'd'}^2(\beta) \times \\
d_{de}^2(\beta) d_{d'e'}^2(\beta) \langle e^{i[b(\phi_1(t)+\pi)-b'(\phi_1(0)+\pi)]}\rangle \langle e^{i[c(\phi_2(t)+\pi)-c'(\phi_2(0)+\pi)]}\rangle \times \\
\langle e^{i[d(\phi_3(t)+\pi)-d'(\phi_3(0)+\pi)]}\rangle \langle e^{i[e(\phi_4(t)+\pi)-e'(\phi_4(0)+\pi)]}\rangle \times \\
Y_e^2(\theta_{mol},\phi_{mol}) Y_{e'}^2(\theta_{mol},\phi_{mol}) \quad \text{(A9)}
\end{aligned}$$

In Section IV, the NMR relaxation parameters obtained from eq A8 and A9 are compared. Appendix C shows how to evaluate the multiple sums that appear in eq A9 by an efficient procedure. The results from a lattice jump model that is an analytically tractable approximation to eq A9 are also presented in Section IV; the specific formulation of the lattice jump model is given in Appendix B.

Appendix B

In this appendix we evaluate the required ensemble averages for the simplest lattice jump model for the alkane internal dynamics. It is assumed that independent jumps are allowed about each backbone bond between the stable trans, gauche (+), and gauche (−) states; the gauche (+), gauche (−) transition is excluded and no additional motions (e.g., oscillations within a well) are included in the model. The required ensemble averages (eq A9) are evaluated from the model by use of the expression (eq 18)

$$\langle e^{i[m\phi(t)-m'\phi(0)]}\rangle = \sum_{\substack{\phi= \\ \tau,g^-,g^+}} \sum_{\substack{\phi'= \\ \tau,g^-,g^+}} e^{i[m\phi-m'\phi']} P(\phi') P(\phi,t|\phi',0) \quad \text{(B1)}$$

where, for example, $P(\tau)$ is the equilibrium probability that the

rotational angle ϕ is trans, and $P(\tau,t|g^+,0)$ is the conditional probability the rotational angle ϕ is trans at time t given that it was gauche (+) at time 0. Wallach[24] and London et al.[29] have presented the conditional probability for this lattice jump model in terms of the rate constants. Here we derive the result from a general approach that constructs the conditional probability from the eigenvectors and eigenvalues of a master equation (see, for example, ref 26). The master equation for this independent lattice jump model is

$$\frac{dN_t}{dt} = -2K_tN_t + K_g[N_{g^+} + N_{g^-}] \tag{B2a}$$

$$\frac{dN_{g^+}}{dt} = K_tN_t - K_gN_{g^+} \tag{B2b}$$

$$\frac{dN_{g^-}}{dt} = K_tN_t - K_gN_{g^-} \tag{B2c}$$

where $N_\phi \equiv N_\phi(t)$ is the probability of finding the system in state ϕ at time t and K_t and K_g are the rate constants for jumping from trans to gauche (+) or (−) states and from gauche (+) or (−) to trans states, respectively. The rate constants satisfy microscopic reversibility; that is,

$$\frac{N_t^\circ}{N_{g^+}^\circ} = \frac{N_t^\circ}{N_{g^-}^\circ} = \frac{K_g}{K_t} \tag{B3}$$

where N_t° and $N_{G^{+(-)}}^\circ$ are the equilibrium fractions of trans and gauche (+) or (−) states. The master equation therefore has a zero eigenvalue ($\lambda_0 = 0$). Subtracting eq B2c from eq B2b we have

$$\frac{d}{dt}[N_{g^+} - N_{g^-}] = \frac{d}{dt}\delta N_g = -K_g\delta N_g;\ \delta N_g(t) = e^{-K_gt}\delta N_g(0) \tag{B4}$$

The second eigenvalue of the master equation is, therefore, $\lambda_1 = K_g$. With use of the conservation equation,

$$N_t + N_{g^+} + N_{g^-} = 1 \tag{B5}$$

Equation B2a can be rewritten in the form

$$\frac{d}{dt}(N_t(t) - N_t^\circ) = \frac{d}{dt}\delta N_t(t) = -(2K_t + K_g)\delta N_t;\ \delta N_t(t) = e^{-(2K_t+K_g)t}\delta N_t(0) \tag{B6}$$

The third eigenvalue of the master equation is, therefore, $\lambda_2 = 2K_t + K_g$. By the substitution $N_\phi(t) = X_\phi e^{-\lambda t}$ and symmetrization, the symmetric matrix equivalent of the master equation[26] is found to be

$$\begin{bmatrix} -2K_t & [K_gK_t]^{1/2} & [K_gK_t]^{1/2} \\ [K_tK_g]^{1/2} & -K_g & 0 \\ [K_tK_g]^{1/2} & 0 & -K_g \end{bmatrix} \chi = -\lambda\tilde{\chi} \tag{B7}$$

where $\tilde{\mathbf{X}}$ is an eigenvector with components $[\chi^\tau, \chi^{g^+}, \chi^g]$. The eigenvectors of eq B7 are

$$\lambda_0 = 0 \qquad \lambda_1 = K_g$$

$$\tilde{\chi}_0 = \begin{bmatrix} \left[\frac{K_g}{2K_t + K_g}\right]^{1/2} \\ \left[\frac{K_t}{2K_t + K_g}\right]^{1/2} \\ \left[\frac{K_t}{2K_t + K_g}\right]^{1/2} \end{bmatrix} \qquad \tilde{\chi}_1 = \begin{bmatrix} 0 \\ \frac{1}{\sqrt{2}} \\ \frac{-1}{\sqrt{2}} \end{bmatrix}$$

$$\lambda_2 = 2K_t + K_g$$

$$\tilde{\chi}_2 = \begin{bmatrix} -\sqrt{2}\left[\frac{K_t}{K_t + 2K_g}\right]^{1/2} \\ \frac{1}{\sqrt{2}}\left[\frac{K_g}{K_t + 2K_g}\right]^{1/2} \\ \frac{1}{\sqrt{2}}\left[\frac{K_g}{K_t + 2K_g}\right]^{1/2} \end{bmatrix} \tag{B8}$$

The eigenvectors are orthonormal and the components of the eigenvector χ_0 have the property

$$(\chi_0^1)^2 = N_t^\circ;\ (\chi_0^2)^2 = (\chi_0^3)^2 = N_{g^+}^\circ = N_{g^-}^\circ$$

The conditional probabilities, $P(\phi,t|\phi',0)$, are solutions to the master equation with delta function initial conditions and can be expanded in terms of the above eigenvalues and eigenvectors; that is,

$$P(\phi,t|\phi',0) = \chi_0^\phi(\chi_0^{\phi'})^{-1}\sum_{n=0}^{2}\chi_n^\phi\chi_n^{\phi'}e^{-\lambda_nt} \tag{B9}$$

In eq B8 and B9, ϕ, $\phi' = \tau$, g^+, and g^- correspond to 1, 2, and 3, respectively. Substituting from the above results, we have

$$P(\tau,t|\tau,0) = \frac{K_g}{2K_t + K_g} + \frac{2K_t}{2K_t + K_g}e^{-(2K_t+K_g)t}$$

$$P(g^+,t|g^+,0) = \frac{K_t}{2K_t + K_g} + \frac{1}{2}e^{-K_gt} + \frac{1}{2}\frac{K_g}{2K_t + K_g}e^{-(2K_t+K_g)t}$$

$$P(g^-,t|g^-,0) = P(g^+,t|g^+,0)$$

$$P(g^+,t|\tau,0) = \frac{K_t}{2K_t + K_g} - \frac{K_t}{2K_t + K_g}e^{-(2K_t+K_g)t}$$

$$P(g^-,t|\tau,0) = P(g^+,t|\tau,0)$$

$$P(\tau,t|g^+,0) = \frac{K_g}{2K_t + K_g} - \frac{K_g}{2K_t + K_g}e^{-(2K_t+K_g)t}$$

$$P(\tau,t|g^-,0) = P(\tau,t|g^+,0)$$

$$P(g^-,t|g^+,0) = \frac{K_t}{2K_t + K_g} - \frac{1}{2}e^{-K_gt} + \frac{1}{2}\frac{K_g}{2K_t + K_g}e^{-(2K_t+K_g)t}$$

$$P(g^+,t|g^-,0) = P(g^-,t|g^+,0) \tag{B10}$$

We note that $P(g^-,t|g^+,0)$ is not zero even though the direct rate constants for jumping from g^+ to g^- are zero. Also, the conditional probabilities have the long-time behavior:

$$P(\tau,\infty|\phi',0) = N_t^\circ \qquad P(g^+,\infty|\phi',0) = N_{g^+}^\circ \qquad P(g^-,\infty|\phi',0) = N_{g^-}^\circ \tag{B11}$$

The conditional probabilities (eq B10) were used to calculate the ensemble averages (eq B1) for the independent lattice jump model. The ensemble averages form a 5 × 5 matrix; however, there are only four independent matrix elements:

$$\langle e^{i[m\phi(t)-m'\phi(0)]}\rangle =$$

$$1 \quad \text{if } m = m' = 0$$

$$\frac{K_g - K_t}{K_g + 2K_t} \quad \text{if } m = 0 \text{ and } m' \neq 0 \text{ or } m \neq 0 \text{ and } m' = 0$$

$$\left[\frac{K_g - K_t}{K_g + K_t}\right]^2 + \frac{3}{2}\frac{K_t}{K_g + 2K_t}e^{-K_gt} + \frac{9}{2}\frac{K_tK_g}{(K_g + 2K_t)^2}e^{-(2K_t+K_g)t}$$

if $m = m' \neq 0$
or $m = \mp 1$ and $m' = \mp 2$
or $m = \pm 2$ and $m' = \mp 1$

$$\left[\frac{K_g - K_t}{K_g + 2K_t}\right]^2 - \frac{3}{2}\frac{K_t}{K_g + 2K_t}e^{-K_gt} + \frac{9}{2}\frac{K_tK_g}{(K_g + 2K_t)^2}e^{-(2K_t+K_g)t}$$

if $m = -1$ and $m' = 2$ or $+1$
$m = +1$ and $m' = 1$ or $+2$
$m = +2$ and $m' = -2$ or $+1$
$m = -2$ and $m' = -1$ or $+2$ (B12)

Given the ensemble averages (eq B12) and the values of the rate constants K_t and K_g (in the present calculations obtained from the stochastic dynamic trajectory[34]), the independent lattice jump model correlation functions in eq A9 can be evaluated.

Appendix C

In the product approximations (eq 17 and A9), the sums that must be calculated to evaluate the time correlation functions are quite lengthy. London and Avitable[27,29] have described an algorithm that can be used to reduce the computation time based on the symmetry relations for the reduced Wigner matrices and the symmetry associated with the potential for the rotational motion. To demonstrate what is involved, we show how to reduce the sum required for the C_6 relaxation in the product approximation. In order to use the algorithm, the sum in eq A9 is written in the form

$$\sum_{\substack{abcde\\ b'c'd'e'}} \langle d_{ab}^{2} d_{ab'}^{\prime 2} e^{i[b(\phi_1(t)+\pi)-b'(\phi_1(0)+\pi)]}\rangle \ldots \times$$
$$\langle d_{de}^{2} d_{d'e'}^{\prime 2} e^{i[e(\phi_4(t)+\pi)-e'(\phi_4(0)+\pi)]}\rangle Y_e^{2} Y_e^{*2} =$$
$$\sum_{\substack{abcde\\ b'c'd'e'}} [(-1)^{a-a'} d_{ab}^{2} d_{ab'}^{2}][(-1)^{b-b'} d_{bc}^{2} d_{b'c'} \langle e^{i(b\phi_1(t)-b'\phi_1(0))}\rangle] \times$$
$$[(-1)^{c-c'} d_{cd}^{2} d_{c'd'}^{2} \langle e^{i(c\phi_2(t)-c'\phi_2(0))}\rangle] \times$$
$$[(-1)^{d-d'} d_{de}^{2} d_{d'e'}^{2} \langle e^{i[d\phi_3(t)-d'\phi_3(0)]}\rangle] \times$$
$$[(-1)^{e-e'} d_{e0}^{2} d_{e'0}^{2} \langle e^{i[e\phi_4(t)-e'\phi_4(0)]}\rangle \cos([e-e']\phi_{mol}) (5/4\pi) \quad (C1)$$

We have suppressed all the β angles and used the fact that

$$R_e[Y_e^{2}(\theta_{mol},\phi_{mol}) Y_{e'}^{2*}(\theta_{mol},\phi_{mol})] = [d_{e0}^{2} d_{e'0}^{2} \cos([e-e']\phi_{mol})(5/4\pi)] \quad (C2)$$

since only the real part contributes to the sum.

The four-dimensional arrays are introduced

$$N_{ii'jj'} = (-1)^{i-i'} d_{ij}^{2} d_{i'j'}^{2} \quad (C3)$$

and used to express the sum, eq C1, as

$$\frac{5}{4\pi} \sum_{\substack{abcde\\ b'c'd'e'}} N_{aabb'}[N_{bb'cc'}\langle e^{i[b\phi_1(t)-b'\phi_1(0)]}\rangle][N_{cc'dd'}\langle e^{i[c\phi_2(t)-c'\phi_2(0)]}\rangle] \times$$
$$[N_{dd'ee'}\langle e^{i[d\phi_3(t)-d'\phi_3(0)]}\rangle][N_{ee'00}\langle e^{i[e\phi_4(t)-e'\phi_4(0)]}\rangle] \cos[(e-e')\phi_{mol}] \quad (C4)$$

Since not all the terms in this sum are distinct,[27,30] it is convenient to combine equivalent terms by use of the additional four-dimensional array,[27,30]

$$M_{ii'jj'} = N_{ii'jj'} + (i-\delta_{j-j'})(-1)^{j+j'} N_{ii-j'j} + (1-\delta_{jj'})[N_{iij'j} + (1-\delta_{j-j'})(-1)^{j+j'} N_{ii'-j-j'}] \quad (C5)$$

In terms of this array the required time correlation function can be rewritten

$$\langle Y_0^{2}(\theta(t)\phi(t)) Y_0^{2*}(\theta(0)\phi(0))\rangle = \left(\frac{1}{4\pi}\right) e^{-t/t_0} \sum_{a=0}^{2} \sum_{\substack{bcde\\ =0}}^{2} \sum_{b'=-b}^{b} \sum_{c'=-c}^{c} \sum_{d'=-d}^{d} \sum_{e'=-e}^{e} [C_a M_{aabb'}] \times$$
$$[M_{bb'cc'}]\ \langle e^{i[b\phi_1(t)-b'\phi_1(0)]}\rangle][M_{cc'dd'}\langle e^{i[c\phi_2(t)-c'\phi_2(0)]}\rangle] \times$$
$$[M_{dd'ee'}\langle e^{i[d\phi_3(t)-d'\phi_3(0)]}\rangle] \times$$
$$[M_{ee'00}\langle e^{i[e\phi_4(t)-e'\phi_4(0)]}\rangle] \cos([e-e']\phi_{mol}) \quad (C6)$$

where $C_0 = 1$ and $C_1 = C_2 = 2$. The time correlations required to compute this sum, $\langle e^{i(m\phi(t)-m'\phi(0))}\rangle$, can be obtained either from the trajectory or from simplified models. In order to evaluate the time correlation of the spherical harmonics for atom C_6 at 100 points in time, the symmetry relations have been used to reduce the sum from 195 000 000 terms (eq C1) to 1 970 000 terms (eq C6). Equation C6 was verified by comparison with eq C1 for the first few time increments. The cost of computing the correlation functions for a chain much longer than heptane becomes prohibitively expensive, even when the summation is simplified as described here.

Paramagnetic Doping as an Aid in Obtaining High-Resolution ^{13}C NMR Spectra of Biomolecules in the Solid State

S. Ganapathy, A. Naito, and C. A. McDowell*

Contribution from the Department of Chemistry, University of British Columbia, Vancouver, British Columbia, Canada V6T 1Y6. *Received January 12, 1981*

Abstract: Introduction of a paramagnetic impurity is shown to be an effective method in obtaining ^{13}C cross-polarization magic angle spinning (CP–MAS) spectra of biomolecules in the solid state. When doped with Cu^{2+} as a paramagnetic impurity, ^{13}C spectra of imidazole, uracil, thymine, and cytosine·H_2O could be easily obtained. But their spectra in the pure compounds were far too difficult to obtain because of the long proton spin–lattice relaxation times. It is also confirmed that a moderately low amount of paramagnetic species (Cu^{2+} molar concentration $\lesssim$ 0.4% used in the present study) does not produce any observable shift or broadening of the ^{13}C resonances, thereby preserving the quality of the spectra. The spectra so obtained exhibit features peculiar to the solid state. The solid state ^{13}C CP–MAS spectrum of imidazole reveals three distinct ^{13}C resonances, as against two in solution, because of the freezing out of tautomerism.

Sensitivity enhancement by cross-polarization (CP)[1,2] and resolution enhancement by dipolar decoupling[2] and magic angle spinning (MAS)[3,4] have made it possible to obtain high-resolution, natural-abundance ^{13}C NMR spectra in the solid state.[5] The main advantage of using CP–MAS technique rests with the fact that the repetition time of the experiment, while signal averaging, is essentially determined by a shorter proton spin–lattice relaxation time (T_1^H) compared to a much longer carbon spin–lattice relaxation time (T_1^C). But T_1^H can be very long (greater than 100 s) in the extreme correlation limits, viz., $\omega_{OH}\tau_C >> 1$ (very slow motion) and $\omega_{OH}\tau_C << 1$ (very fast motion), rendering a CP–MAS experiment to be of low sensitivity. Therefore it becomes necessary to device means by which T_1^H can be reduced and a ^{13}C spectrum easily obtained with a gain in detection sensitivity.

The utility of introducing a paramagnetic impurity into a host lattice with a subsequent reduction in T_1^H is well known.[6,7] With

(1) Hartmann, S. R.; Hahn, E. L. *Phys. Rev.* **1962**, *128*, 2042–2053.
(2) Pines, A.; Gibby, M. G.; Waugh, J. S. *J. Chem. Phys.* **1973**, *59*, 569–590.
(3) Andrew, E. R.; Bradbury, A.; Eades, R. G. *Nature (London)* **1958**, *182*, 1659.
(4) Lowe, I. J. *Phys. Rev. Lett.* **1959**, *2*, 285–287.
(5) Schaefer, J.; Stejskal, E. O. *J. Am. Chem. Soc.* **1976**, *98*, 1031–1032.
(6) Bloembergen, N. *Physica (Amsterdam)* **1949**, *15*, 386–426.
(7) Gennes De, P-G. *Phys. Chem. Solids*, **1958**, *7*, 345–350.

0002-7863/81/1503-6011$01.25/0